The Synthesis, Characterization and Modification of Gold Nanoparticles for use in SERS-based COVID-19 Antibody Testing

by

© Marissa J. MacInnis, 2021

An Honours thesis submitted to Saint Mary's University in partial fulfillment of the requirements for the degree of

Certificate of Honours Equivalency

Department of Chemistry

Saint Mary's University

6 April 2021

Halifax, Nova Scotia

Certification

The Synthesis, Characterization and Modification of Gold Nanoparticles for use in SERS-based COVID-19 Antibody Testing

By: Marissa J. MacInnis

I hereby certify that this thesis was completed by Marissa J. MacInnis in partial fulfillment of the requirements of the Certificate of Honours Equivalency in Chemistry at Saint Mary's University and I certify that this is truly the original work carried out by Marissa J. MacInnis.

Thesis Supervisor:

Dr. Christa L. Brosseau

Chairperson of the Chemistry Department

Dr. Jason Masuda

Date: April 2021

Abstract

The current COVID-19 pandemic has highlighted a need for rapid, point-of-care (POC) antibody testing. Antibody testing would allow for a determination of which members of the population have already been infected with the SARS-CoV-2 virus, and also which members have built up sufficient immunity after vaccination. Current POC diagnostic platforms which screen for antibodies in bodily fluids are typically either lateral flow or vertical flow based, and make use of labelled colloidal gold, which exhibits a red colour, as the visual interpretation for the test. In this thesis work, we are seeking to use the colloidal gold in these platforms as the enhancing element in surface-enhanced Raman spectroscopy (SERS) which would make such tests not only qualitative but also quantitative. For SARS-CoV-2 infections, this means that antibody levels could be monitored over time, which would be very useful. In this work, colloidal gold nanoparticles (AuNP) were synthesized, characterized and modified for use in such rapid test platforms. The AuNPs of varying diameters were characterized using UV-Vis and scanning electron microscopy. The SERS performance of the AuNPs was ascertained using a probe molecule as a tag. The AuNPs were modified with a capture agent and the SERS tag components, and were explored for use in a flow assay prototype. These results indicate that modified AuNPs in conjunction with SERS may be useful for quantitative readouts for COVID-19 antibody testing platforms.

Acknowledgements

Firstly, I would like to thank my honours thesis supervisor, Dr. Christa Brosseau, for your support and guidance throughout my time at Saint Mary's University, and for allowing me to the opportunity to complete my honours thesis in your research lab. I would like to thank the Brosseau lab group members for their advice and sharing of expertise. Next, I would like to thank Dr. Xiang Yang, for taking the time to help me obtain SEM images and providing SEM training. Finally, I want to thank my friends and family, especially my brother, for their support throughout my undergraduate studies. John, thank you for your continued encouragement throughout my undergraduate degree and honours thesis. Your guidance and knowledge in and beyond chemistry has been instrumental for *any and all of my accomplishments.*

Table of Contents

List of Symbols and Abbreviations

4-ATP	4-aminothiophenol
AuNP	Gold nanoparticle
AuNS	Gold nanostar
BSA	Bovine serum albumin
FE-SEM	Field-emission scanning electron microscope
hCG	Human Chorionic Gonadotrophin
HCl	Hydrochloric acid
HNO_3	Nitric acid
IgG	Immunoglobulin G
LFA	Lateral flow assay
LFIA	Lateral flow immunochromatographic assay
$NaHCO_3$	Sodium bicarbonate
NP	Nucleoprotein
PCR	Polymerase chain reaction
POC	Point-of-care
PPE	Personal protective equipment
PYOT	5-(4-Pyridyl)-1,3,4-oxadiazole-2-thiol
rNP	Recombinant nucleoprotein
rpm	Revolutions per minute
SARS	Severe Acute Respiratory Syndrome
SARS-CoV-2	Severe acute respiratory syndrome coronavirus 2
SEM	Scanning electron microscope
SERS	Surface enhanced Raman spectroscopy
TEM	Transmission electron microscope
UV-Vis	Ultraviolet-Visible Spectroscopy

List of Figures

List of Tables

Introduction

Overview of COVID-19

A novel disease known as COVID-19 has recently surfaced as a result of a new strain of coronavirus. On March 11, 2020, COVID-19 was declared a global pandemic by the World Health Organization. The virus responsible for COVID-19 is the severe acute respiratory syndrome coronavirus 2 (SARS-CoV-2). COVID-19 is a respiratory disease and is related to the family of viruses that cause Severe Acute Respiratory Syndrome (SARS) and some viruses related to the common cold. The namesake of the new virus strain comes from the genetic similarities to the coronavirus strain that caused the SARS outbreak in 2003.[1] Several symptoms of COVID-19 may present in infected individuals, including a cough, fever, difficulty breathing, among others. COVID-19 can be fatal and has a higher mortality rate for at risk populations, such as elderly individuals and those with chronic medical conditions or otherwise compromised immune systems. Some of the underlying medicals conditions that may place people in a higher risk category include cancer, cardiovascular disease, diabetes, among others.[2] While fighting a COVID-19 infection, both the innate and acquired immune system are required. For populations who have weakened immune systems or those who are immunocompromised, the activation of the acquired immune system may be delayed, which can explain the higher mortality and morbidity of COVID-19 in those populations. When individuals of higher risk groups contract COVID-19, along with a higher mortality rate, they may be more prone to developing serious symptoms of COVID-19 with long-term effects. Additionally, in approximately 80% of all cases, infected individuals recover without the need for medical intervention, and experience mild illness similar to common influenza.[3]

The spread of COVID-19 can be slowed or prevented altogether by wearing masks, washing hands often with soap and warm water, staying home when sick, among other things. Fabric and disposable medical masks have been recommended for the general public, and the N95 mask should be reserved for healthcare professionals.[4] Studies have been conducted which demonstrate the effectiveness of masks in protecting against the transmission of COVID-19. Konda et al. studied the aerosol filtration efficiency of common fabrics used in respiratory cloth masks and N95 masks.[5] This study completed by Konda et al. is one example of a multitude of studies and research that has been completed relating to the COVID-19 pandemic.

Several vaccines for COVID-19 have recently been evaluated and approved in Canada. To date, Moderna, Pfizer-BioNTech, AstraZeneca, and Janssen have had vaccines approved for use and other vaccines are currently under review. The Moderna and Pfizer-BioNTech vaccines are mRNA vaccines. The mRNA vaccines provide information to cells on how to synthesize proteins that trigger an immune response against the SARS-CoV-2 virus without using the live virus that causes COVID-19. Once the immune response is triggered, antibodies are made, which can help the body fight an infection if the SARS-CoV-2 virus does infect the body in the future.[6,7] The AstraZeneca and Janssen vaccines are viral vector-based vaccines. With the AstraZeneca and Janssen vaccines, an adenovirus is used as a delivery system, which is a type of harmless virus. The vector virus produces the SARS-CoV-2 spike protein, which is found on the surface of the SARS-CoV-2 virus. The body is able to recognize this protein as foreign and builds an immune response against the spike protein without ever having been exposed to the SARS-CoV-2 virus.[8,9] The various vaccine types listed provide varying degrees of efficacy, but all vaccines demonstrate a significant reduction in hospitalizations and deaths. Vaccination is important

for the development of herd immunity in a population. Before the vaccines are readily available to the majority of the population, it is important to remain vigilant in preventing the spread of COVID-19 by taking preventative measures such as wearing masks and washing hands often to avoid transmission of the virus.

The transmissibility of the SARS-CoV-2 virus has been studied extensively since the onset of the pandemic. Kawasuji et al. found that the viral load plays an important role in the transmission of COVID-19.[10] The viral load refers to the amount or concentration of a virus in an infected individual's blood. Higher viral loads were linked to severe COVID-19 cases and lower viral loads were linked to milder cases of COVID-19. Treatment of COVID-19 can vary greatly between cases, and in severe cases with high viral loads, steroid treatments may be recommended rather than antiviral.[11] This demonstrates the importance of quantitative rather than qualitative viral testing methods, as the viral concentrations can impact treatments when warranted.

Various testing methods are used for the diagnosis of COVID-19. Polymerase chain reaction (PCR) tests, which are also called molecular tests, function by detecting genetic material of the SARS-CoV-2 virus and are considered the gold standard in viral diagnostics. Samples are collected via nasal swabs or throat swabs, and sometimes saliva samples are collected from tubes, for testing. Result time may vary depending on whether or not the test is being processed onsite (rapid testing) or if testing is taking place offsite in a laboratory. Offsite testing may take days or longer depending on the location of the test processing site and other processing delays, such as large testing volumes. PCR tests are generally very accurate. The rapid viral testing method is less accurate than PCR tests and may miss some positive cases, or result in false positive tests. Usually, positive rapid test results are confirmed via offsite laboratory PCR testing, due to their high accuracy.[12,13]

Antigen testing is another testing method used for COVID-19 diagnosis. Antigen tests function by detecting proteins associated with the SARS-CoV-2 virus. Nasal swabs can be used to collect samples and rapid test results are available quickly where onsite test processing is available. Similar to PCR testing, samples for antigen testing may be processed offsite in a laboratory for analysis, with longer processing times. False negative test results occur at a higher rate with antigen tests than PCR tests. As a result, a PCR test may be recommended to confirm a negative antigen test result.[13] COVID-19 testing is important for a number of reasons. Individuals who test positive and need treatment can get treatment earlier. Increased testing allows for increased contact tracing for confirmed positive cases, which can lead to less transmission as confirmed contacts can quarantine. Isolating confirmed cases and close contacts can help prevent future outbreaks of the disease. Further, testing can help track the number of individuals who are infected in an area, which provides information concerning the level of risk in a community. Testing data can impact public health guidelines in communities.[14] No existing technology can provide 100% accurate test results, so it is important to follow public health guidelines regardless of COVID-19 diagnostic test results.

Antibody Testing

As a result of the current COVID-19 pandemic, rapid and reliable tests are necessary in order to track individuals who have been infected with, and have immunity to, the novel coronavirus. Antibody testing, also known as serology testing, is typically completed following a recovery from COVID-19. The tests typically function by taking a blood or other serological sample and testing the sample to verify whether or not antibodies

exist in a sample, which would indicate antibodies have been developed against the virus after infection. Positive antibody tests indicate that antibodies have been produced in the body as a result of a past infection with COVID-19 or due to vaccine efficacy, and also indicate some degree of immunity.[15] Studies are ongoing to determine whether antibodies protect against reinfection from COVID-19, the length of time immunity lasts, and the level of immunity provided. The timing of antibody testing is important since testing too early in an infection may not detect antibodies, so it is recommended to test for antibodies no earlier than 14 days after symptoms are observed. Along with indicating how many people have recovered from COVID-19, including those who may not have had symptoms, and determining those who may have immunity, antibody testing can help determine those who may be eligible to donate plasma. Plasma donations for COVID-19 can function to treat others with severe cases of the disease and boost their ability off fight off the coronavirus.[13]

To date, various antibodies of SARS-CoV-2 have been studied, along with their characteristics. There are three relevant classes of antibodies of concern while considering human infections and immunity. These antibody classes include IgM, IgG, and IgA, and total antibody count is also a worthwhile datum while considering SARS-CoV-2 antibodies and are often results of interest of COVID-19 serology tests. Briefly, the IgM antibody is one of the first antibodies produced and able to be detected during a COVID-19 infection. The IgM antibody exists in the bloodstream as a pentamer, where five of the IgM antibodies join together in a ring form. This antibody is the largest by size found in the body, however it makes up only 10% of the total antibody count. IgG in comparison is the most abundant in the bloodstream, making up 80% of the total antibody count. IgG is the smallest antibody and exists as a monomer. IgG presents later on in a COVID-19 infection, when mature B cells of the immune system signal the switch from production of IgM to IgG. IgG is highly

specific and long-lasting in the immune system, which makes IgG an important antibody while working towards long-term immunity post infection. Finally, the IgA antibody exists as a dimer in the secretory system. The IgA antibody comprises a small portion of the total antibody count.[16] Studies are ongoing to determine the decline of SARS-CoV-2 antibodies over time following acute infection. For example, one study found that over one quarter of individuals who had been infected with COVID-19 tested serologically negative approximately 60 days after initial serological testing for COVID-19. The observed decline in antibody levels may not indicate a loss of protective immunity or an increased risk of infection, and must be studied further.[17] Finally, a decline in antibody levels overtime could relate to the requirement of booster vaccinations, in an effort to maintain high antibody levels over time.

Technology already exists, and some technology is currently in development, to test whether individuals have already been infected with and therefore have some immunity for COVID-19. Briefly, a lateral immunoassay test could be modified in order to act as a COVID-19 antibody test. The modifications may take place on a common lateral flow immunoassay test, for example, a store-bought take-home pregnancy test, as well as a more advanced test kit. The lateral flow immunoassay tests can be used to detect various antibody target molecules. Commercial test kits have been developed for the SARS-CoV-2, which allow for at-home testing. Test results may be acquired for clinical and research uses, including studies concerning COVID-19 infection rates at specific community levels.[17] Carter et al. describe various assay techniques and tests possible for use in COVID-19 antibody testing. Highlighted in their literature are increasing trends relating to diagnostic and serological tests for COVID-19.[17] Much of the existing commercial test kit

development that allows for at-home testing was based on content in this literature, including lateral flow assay tests.

Since the majority of rapid testing platforms, including lateral flow (LF) and rapid vertical flow (RVF) assays use gold nanoparticles modified with capture agent as the visual readout, it makes sense to couple such platforms with spectroscopic techniques which rely on these noble metal nanoparticles. One example of such a platform is surface-enhanced Raman spectroscopy (SERS). In SERS, the Raman signal is magnified by one million-fold when the analyte of interest is on, or in very close proximity to a nanostructured coinage metal surface (Au, Ag, Cu). Gold nanoparticles may be conjugated with Raman reporters (molecules which exhibit large Raman cross-sections), surface coating(s), and surface ligands to form a particle for use in antibody testing. Raman reporters will enable quantitation of antibodies present and allow for greater sensitivity.[18] Protein A is a surface ligand that may be coupled with Raman reported molecules and noble metal particles for use in SERS and allows the binding antibody to be anchored to the gold nanoparticle. The SERS technique is highly sensitivity, therefore it is the method of choice in this thesis project. In future research projects, the lateral flow immunoassay test coupled with SERS could be paired with a portable readout tool, and provide quantitative information concerning antibody concentrations and other valued information. This would also provide the user with positive or negative (qualitative) information regarding testing. By developing this existing technology, we could improve the quality of testing completed. This will be useful for applications relating to the COVID-19 pandemic, and potentially future viral illnesses that are contagious and require rapid or home testing.

In the last number of months, there has been an increased demand for the development of point-of-care (POC) testing devices for diagnostic purposes as a result of

the novel coronavirus pandemic. It is important that these testing devices have high sensitivity and specificity for the target molecule. An overview of current technologies being developed for diagnostic purposes includes magnetic, fluorescent, electrochemical, and flow assay technologies, among others.[19] For example, magnetic nanoparticles that have been developed by Zhao et al., are coated with poly-carboxyl for the detection of SARS-CoV-2 RNA.[20] Similar magnetic nanoparticles have been conjugated with antibodies. The particles would self-assemble in the presence of the viral target molecule which resulted in structures with enhanced magnetic properties. The enhanced magnetic properties allowed for detection of these molecules by magnetic resonance methods such as NMR or MRI.[21] Further, Wang et al. proposed a magnetic SERS strip which has shown rapid operation, stability, high specificity, and reproducibility. The magnetic SERS nanocomposite functions similarly to typical SERS tags, with a key difference in separating target molecules magnetically. Overall, the drawback of low sensitivity has limited the use of magnetic sensors to date.[22] Colorimetric and fluorescent sensors are often coupled with other assay tests. They are spectral detection methods in which a spectral change indicates the presence or absence of a target molecule.[19] Colorimetric sensors offer limited sensitivity, and fluorescent sensors rely on expensive and labile fluorophores, therefore, both of which are not ideal, and their use is limited. Further, electrochemical biosensors have been developed which observe changes in resistivity or capacity in order to detect target molecules. The lateral flow immunochromatographic assay (LFIA) has become a key technology and a useful tool for rapid screening due to its simplicity and compatibility with other applications.[23]

Typically, LFIA test interpretation is based on colour visualization using colloidal gold nanoparticles. It may be coupled with SERS, which is an analytical technique which

may be used in order to improve normal Raman scattering. SERS can enhance the detection of single molecules by a magnitude of 10^{10} to 10^{11} compared to normal Raman.[18] Combination of SERS and LFIA techniques have been developed and reported on in the literature. These LFIA-SERS systems used in combination overcome the limitations of each technique separately. For example, the use of SERS improves sensitivity of measurements, which is a drawback of LFIA systems used independently. Typically, LFIA systems used without enhancement offer low sensitivity. Although the mechanism of enhancement is not fully understood, enhancement is generally attributed to molecular absorption of Raman-active reporter molecules, which coat the silver or gold metallic surfaces that act as SERS tag substrates. Generally, the SERS tag consists of a substrate, reporter, surface coating, and surface ligand, with various material options for each component, allowing for optimization concerning specific experimental conditions.[18]

Maneeprakorn et al. developed a LFIA-SERS test system for sensitive influenza detection.[24] SERS was chosen in this study as an alternative signal measurement technique to optical or fluorescence readers, which lack precision of signal measurement conventionally.[25] In this study, engineering of the SERS tag included a gold nanoparticle substrate. Although silver nanoparticles produce higher extinction coefficients than gold nanoparticles, they were not used because they are not highly stable under biological conditions. Rather than spherical particles, multi-branched nanostars were used as it was reported that the geometry would result in higher SERS activity. The increased SERS signal results from the increased surface area nanostars offer compared to nanospheres. The increased surface area offers additional space for the electromagnetic field, which is attributed to the increased SERS signal that results during analysis, compared to Raman spectroscopy without enhancement. However, nanostars have a lower long-term stability

in comparison to nanospheres and will often revert to nanospheres.[26] Therefore, the choice to use nanostars may have been unnecessary and nanospheres would have been adequate. Maneeprakorn et al. used the Frens method to produce the spherical gold nanoparticles. In the standard Frens method, AuNPs are synthesized from $HAuCl_4$ and sodium citrate.[27] The resultant particles were used as the gold seed in the Perrault and Chan synthesis process. Briefly, in the Perrault and Chan process, the gold seed solution is diluted, stirred with heat, and stabilized by the addition of a trisodium citrate solution among several other compounds. Overall, AuNPs were synthesized using an aqueous synthesis via a reduction of a gold salt through a seed-mediated growth approach which included hydroquinone as a reducing agent.[28]

Maneeprakorn et al. used 4-aminothiophenol (4-ATP) as the Raman reporter molecule in this study, and it was covalently attached to the surface of the nanosphere substrate. A number of types of Raman reporter molecules exist in the literature for similar applications. These include nitrogen-containing cationic dyes, sulfur-containing dyes, thiolated molecules, among others.[18] This is due to the high affinity of nitrogen, and sulfur-containing molecules to gold. A strong interaction between a Raman reporter and metal substrate is required in order to avoid desorption during Raman analysis, which could result in spectral interferences.[19] It is also important that the Raman reporter SERS peak does not interfere or overlap with other signals. A selection of common Raman reporter molecules is listed in Table 1.

Table 1. These are several commonly used Raman reporter molecules used in SERS tag preparation and some of their characteristics.[18]

Type	Example	Advantages	Disadvantages
Nitrogen-containing cationic dye	Crystal violet	Low cost	Weak affinity to metal nanosubstrate
Sulfur-containing dyes	Malachite green isothiocyanate	Strong affinity to metal nanosubstrate	Limited options
Thio-small molecules	4-aminothiophenol	Low cost	Small Raman cross section

In the Maneeprakorn et al. study, their result was a gold nanostar-ATP (AuNS-ATP) SERS tag which required antibody conjugation. The preparation of the SERS tag and an overview of the SERS-LFIA test system is outlined in Figure 1. The monoclonal antibody (mAb) specific to nucleoprotein (NP) was conjugated to the AuNS–ATP. This was done using a physical adsorption coupled with buffer method. This conjugation method using the Tris-HCl buffer was also applied in a study completed by Huang et al. on SERS-LFIA detection of SARS-CoV-2 antibodies.[29] Maneeprakorn et al. developed a LFIA strip consisting of 4 components, which included a sample pad, a conjugate pad, a fluid-flow nitrocellulose membrane, and an absorbent pad. The LFIA components were individually purchased and assembled. Tomás et al. conducted research using a LFIA development kit. The kit contained various components, including several types of nitrocellulose membranes with different protein binding capacities, two types of glass fibre sample pads, and two conjugate pads, and the given component options would come with various treatments and buffers, in order to optimize their test strip.[30] Tomás et al. had more optimal methodology in their study in LFIA test strip production compared to Maneeprakorn et al. by allowing additional test component parameters to be exchanged for test strip optimization.

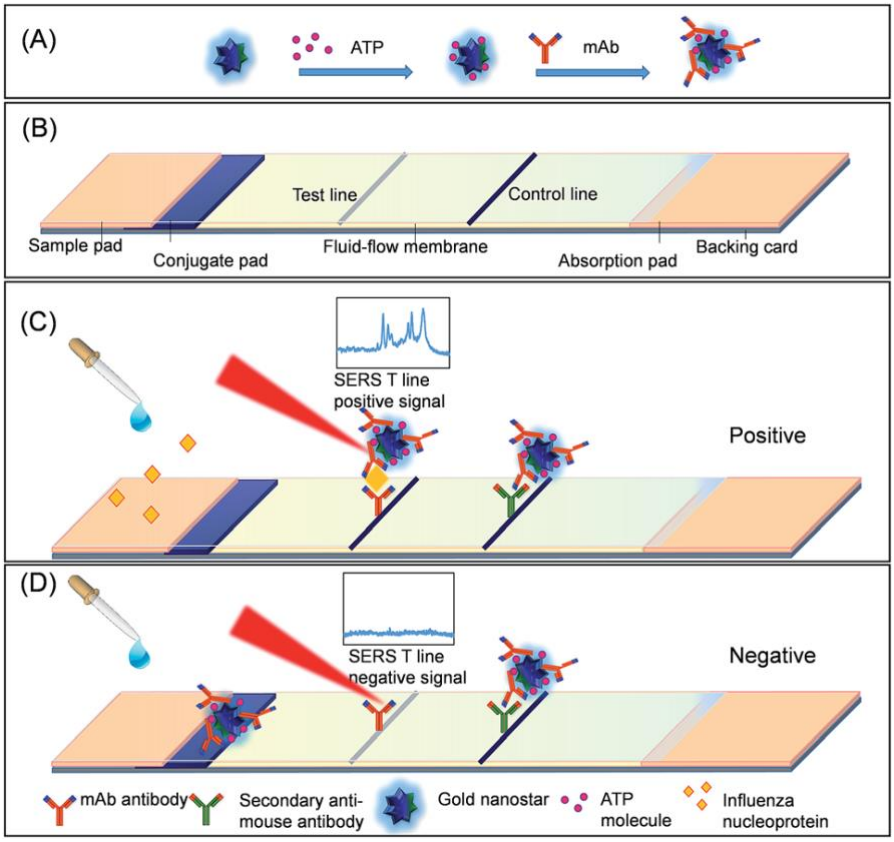

Figure 1. Illustrated above is the SERS-LFIA test system, including (A) SERS tag preparation, (B) the LFIA test, (C) positive, and (D) negative influenza A test results. Figure used with permission from Royal Society of Chemistry.

Maneeprakorn et al. used a number of methods for the characterization of AuNS and AuNS conjugates which gave valued information and ought to be considered for use while developing LFIA-SERS based tests. The AuNS optical response was measured in this study using a microplate spectrophotometer. A transmission electron microscope (TEM) was used to determine the structure and morphology of the AuNS. A field-emission scanning electron microscope (FE-SEM) was used in order to obtain images of the SERS tag in the LFIA membrane. Additionally, Huang et al. used TEM to characterize the structure of their AuNPs in a comparable study using LFIA-SERS technology in order to detect SARS-CoV-2 antibodies. These characterization methods have been consistent with recent literature. Xiao et al. used scanning electron microscopy (SEM) rather than TEM to

determine the structure and morphology of nanostructures in their SERS-LFIA study.[31] The differences between SEM and TEM methods are relatively minor and primarily stem from changes in sample preparation rather than results with TEM requiring a more extensive sample preparation step.

Finally, Maneeprakorn et al. performed the assay test by introducing a 100 μL sample liquid on a sample pad of the test strip. The target molecule was influenza A (H1N1) nucleoprotein in this study. Signal visualization was performed after 15 minutes, which is not an uncommon timeframe for visual results in LFIA testing. A positive test result appears when both a test and control line are visible, while a negative test result appears when solely a control line is visible, as illustrated in Figure 1. The presence of a test line without a control line, or a lack of both test and control lines, indicated inconclusive or invalid results. SERS measurements of the test and control lines were performed using a Raman spectrometer. The sensitivity of the test system was evaluated using various concentrations of the recombinant nucleoprotein (rNP). Maneeprakorn et al. defined the lower limit of detection as the lowest concentration of the rNP that produces a positive test line signal by both visual detection and SERS measurement detection. Liu et al. followed similar limit of detection methods in their SERS based LFIA study on the detection of SARS-CoV-2 antibody samples. Also included were standard IUPAC method LOD calculations.[32] Maneeptakorn et al. evaluated specificity of the test system using a number of other proteins closely related to influenza A, including amicase, avidin, BSA, lysozyme, and tryptone. The results indicated high specificity for the influenza A nucleoprotein against the other proteins. The solutions of AuNS, AuNS–ATP, and AuNS–ATP–mAb were analysed with Raman spectroscopy in order to verify that the particles can be used as a SERS reporter in

the SERS-LFIA test system. The SERS tag also demonstrated a strong Raman signal after conjugation with the antibody.[24] This is an excellent result if future quantification of results is to be considered.

Brosseau et al. developed a point-of-care testing platform for the detection of hepatitis C virus (HCV) antibodies. Rapid vertical flow (RVF) immunotechnology was used in this study and tends to offer low sensitivity and has a limited capacity for quantitative analysis. Due to these limitations, RVF technology was coupled with SERS to improve sensitivity and allow for quantitative information to be gathered from tests. The AuNPs were used as the noble metal nanosubstrate in the SERS tag, and para-aminothiophenol was the Raman reporter molecule used in this study. High quality SERS spectra were obtained in this study which were reproducible and had few interferences. This offered promising results for the use of RVF testing coupled with SERS for biomolecule detection.[33] Further, this study is of particular interest in this thesis work, as the platforms have close similarities.

After considering existing literature and theory, initial steps may be taken in the process of developing a SERS based LFIA test for SARS-CoV-2 antibodies for this thesis work. An existing method may be chosen, or a new method developed for the synthesis of AuNPs, an ideal noble metal nanosubstrate for SERS analysis involving biomolecules. The synthesized AuNPs require characterization to verify their size and morphology. The characterization methods used for nanoparticles may include UV-Vis spectroscopy, SEM, and TEM. The optimal AuNP size (diameter) for SERS analysis needs to be determined as that information will be required for future research. The optimal size may be determined by analyzing SERS spectra that have been obtained from AuNP SERS analysis with an appropriate Raman reporter molecule. Further particle size analysis may be explored to

determine the relation between particle size and SERS intensity. The particle conjugation process will be completed in order to conjugate the AuNPs to 5-(4-Pyridyl)-1,3,4-oxadiazole-2-thiol (PYOT), Bovine Serum Albumin (BSA), Protein A, along with target ligands. A completed and optimized resultant particle which can act as a SERS tag for SARS-CoV-2 antibodies is the anticipated result from this thesis work, which would have application in SERS-based LFIA testing.

Theory

Raman Spectroscopy

Raman spectroscopy is a vibrational fingerprinting technique used for the characterization of molecules. Spectroscopic techniques, such as Raman spectroscopy, function by perturbing bond vibrations of molecules in question using light.[34] In Raman spectroscopy, monochromatic light typically from a laser source is allowed to interact with matter and the scattered light is collected and analyzed. The scattered is typically collected at either a 90° or 180° angle using a CCD camera.[35] As a result, Raman spectroscopy is considered a scattering technique. This differs from other vibrational spectroscopy techniques, such as infrared spectroscopy, which is an absorption technique.[36] Different types of light scattering can result. The most common form of light scattering is Rayleigh scattering, where scattered photons have the same frequency as incident light. Rayleigh scattering is a type of elastic scattering, where there is no net exchange of energy, and therefore, no useful vibrational information about the molecule. On the other hand, a small proportion of the scattered photons are scattered inelastically, and there is a net energy change of the scattered photon – this inelastic scattering is referred to as Raman scattering. Raman scattering includes both Stokes and anti-Stokes components, as the scattered photons can both lose and gain energy, respectively. The energy level diagrams for the scattering processes are shown in Figure 2.

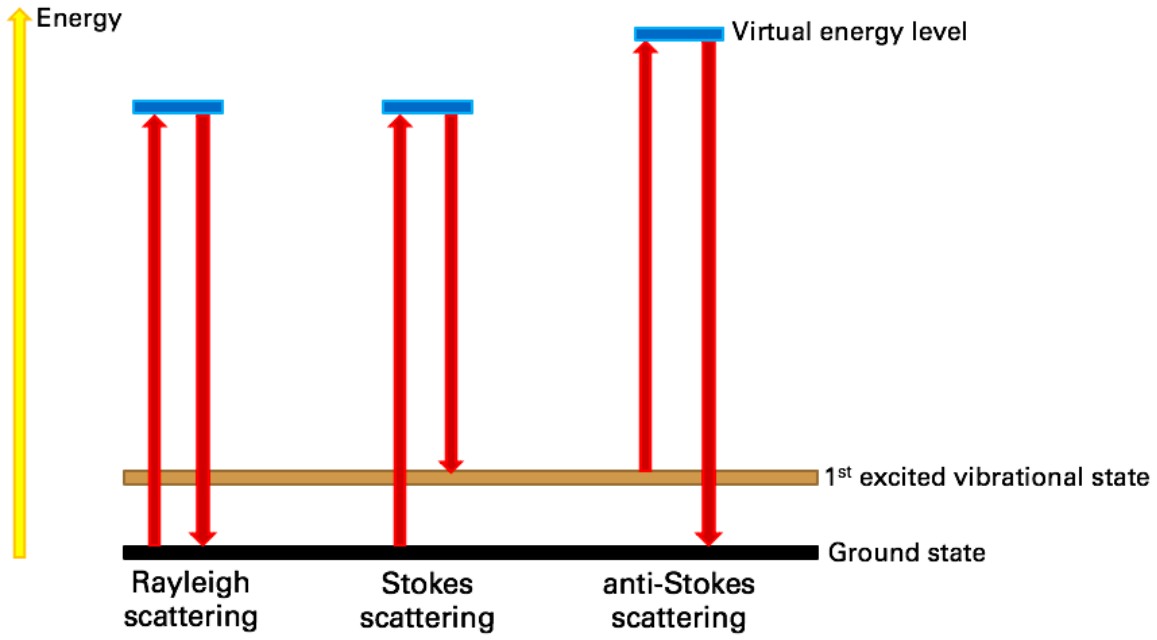

Figure 2. The energy level diagrams for Rayleigh, Stokes, and anti-Stokes scattering.

In Stokes scattering, the scattered light has a lower frequency than the incident light. In anti-Stokes scattering, the light has a higher frequency than the incident light. Most inelastic scattering observed is Stokes scattering, where molecules gain energy.[37] Most Raman spectroscopy analysis is conducted at room temperature, where most molecules are at their lowest vibrational level. Fewer molecules will be at a higher vibrational level than ground state at room temperature. This explains why Stokes scattering is more often observed. The anti-Stokes scattering results from molecules that start at non-zero or non-ground vibrational energy starting points, so the likelihood of this type of scattering occurring is low.[34]

In inelastic scattering, when the incident light interacts with the sample, the electric field component can interact with the electric dipole of the sample. When this occurs, the electron cloud surrounding the bonds in the molecule can become polarized. As a result, inelastic Raman scattering involves changes in the polarizability of bonds. Molecules that

contain bonds that undergo changes in polarizability, and that can be observed via Raman scattering are referred to as Raman active. This is different than other spectroscopic techniques, e.g., infrared spectroscopy, which rely on changes in dipole moment to be produced in order to be considered IR active.[37]

In general, fewer peaks are observed in Raman spectra than IR spectra. This has both advantages and limitations, as Raman spectra tend to be less complicated, but can also provide less information. Differences in the relative strength of peaks can also be observed while comparing Raman and IR spectra. When Raman peaks are strong, IR peaks tend to be weak, and vice versa. Overall, IR and Raman spectroscopy are seen as complimentary techniques.[38] Some additional advantages of Raman spectroscopy over IR include the ability to go to lower wavenumber regions (i.e., down to 50 cm^{-1} is routine) and also the fact that many materials, including water and glass, are weak Raman scatterers.

Raman instrumentation is made up of a laser source, sample cell, wavelength selector, radiation transducer, and a computer for data collection and processing. While analyzing a sample, the sample is first irradiated with laser light. The resultant elastic and inelastic scattered light is filtered in order to eliminate intense elastic Rayleigh scattering as well as weak anti-Stokes Raman scattering. A diffraction grating disperses the filtered light onto the CCD detector where it is then analyzed by a computer program to produce a spectrum.[39] Laser types are chosen based on the laser wavelength. Fluorescence interferences can be observed for Raman spectra. Interferences of this type can be avoided or resolved by changing the laser wavelength to a less energetic wavelength, as Raman shifts are independent of the wavelength of excitation of the laser.[40,41]

Surface-Enhanced Raman Spectroscopy (SERS)

Surface-enhanced Raman spectroscopy is an application of Raman spectroscopy, which enhances Raman scattering by a factor of up to 10^{10} to 10^{11}. SERS uses colloidal or roughened coinage metal surfaces as substrates in the mechanism of increasing signal enhancement.[42] Briefly, the interaction of the oscillating electric field component of light with the metal nanostructures causes a distortion of the free electron density in the metal, and results in a localized EM field at the surface of the metal. This collective oscillation of conduction electrons is referred to as a localized surface plasmon. As a result, adsorbed molecules nearby these metal substrates can exhibit remarkably enhanced Raman signals, down to even single molecule detection levels.[42,43]

Roughened coinage metal surfaces and metal nanoparticles are typically used in SERS analysis because they provide increased surface area where the field can exist and create plasmonic oscillations.[44] The metals used in SERS analysis are typically gold or silver because they have strong plasmonic performance in the visible region of the electromagnetic spectrum. Aluminum, copper, platinum, and palladium have also been explored for use in SERS, with less uptake. The plasmonic response for aluminum is primarily in the UV region, which differs from gold and silver and makes aluminum potentially useful for SERS of biological substances in the future, since most biological molecules have an absorption below 400 nm.[45,46] SERS analysis can be accomplished using colloidal solutions. However, it is more likely that SERS measurements will be performed by putting a liquid sample on a glass or silicon surface which contains a metal nanoparticle coating.[47] There are several considerations to make while considering the formulation of a sample. One consideration concerns the noble metal nanoparticle used at the SERS substrate. The metal choice is important because changes in the metal nanoparticles can

affect the level of enhancement observed while using SERS. Additionally, the size and shape of the nanoparticles affects the ratio of absorption and scattering that occurs, and ought to be considered carefully.[48] The ideal metal nanoparticle substrate would provide high Raman signal intensity enhancement and would be highly uniform. These characteristics lead to SERS sensors which provide signals that are both sensitive and reproducible. A myriad of methods exist for the synthesis of different shapes and sizes of noble metal nanoparticles, and many synthetic strategies allow for excellent control over the size and shape of the metal particles.

SERS can be used to detect a broad range of chemical species, including proteins, enzymes, and other biomolecules. These substances may exist in low quantities in samples and be detected using SERS.[49] Also, given the exceptional sensitivity afforded by SERS, such substrates can be used in applications such as environmental analysis, forensic science, food quality analysis, and pharmaceutical analysis, where the target molecules may exist in low quantity in given samples.[50] Additionally, SERS has applications in immunoassay testing. SERS-based immunoassays can be used to detect various biomolecules in low quantity, with high specificity and selectivity.[51,52] For example, gold nanospheres conjugated with antibodies can be used to detect other antibodies or antigens, through a "sandwich" method, a method of particular interest in this project. Further, based on a SERS spectrum, both quantitative and qualitative information can be gathered relating to the target molecule of interest during analysis.[42]

SERS Tags

SERS tags have been developed for use in Raman analysis as signal boosting entities. SERS tags have typically been made from metal nanoparticles and Raman reporter molecules which offer a strong SERS signal. In more recent advances, SERS tags have been further developed for applications in bioanalysis.[53] A typical SERS tag synthesized for use in bioanalysis is composed of four parts. The components include a metal nanoparticle to act as a SERS substrate, a signal boosting Raman reporter molecule, a blocking agent which functions as a protection shell, and targeting/capture molecules, which may include antibodies or antigens.[18]

SERS tags are made by combining the metal nanoparticle substrate with the Raman reporter molecule, which can be analyzed to see a known SERS spectrum of the tag thus far. Once a spectrum has been observed of the basic tag structure, blocking agents are added to protect the particle, and a biorecognition molecule such as an antibody or antigen is added to give the particle a specific binding feature, along with biocompatibility.[18] These components can be added to the surface of the metal nanoparticle in different orders, and at varying concentrations. When building the SERS tag, it is important to avoid destabilizing the colloidal suspension which causes the metal particles to aggregate and "crash out" of solution. In addition, some SERS tags can be modified with additional layers, such as thin layers of silica, which protect the tag from environmental destabilization.

Other optical probes exist, which include quantum dots and fluorescent dyes. SERS tags offer several advantages over these other optical probes. First, SERS tags offer high enough sensitivity so they can be used for trace analysis of molecules. Also, Raman spectroscopy is more appropriate for advanced analysis because the spectral band width is typically lower than other spectral techniques, such as fluorescence. Therefore, this would

make SERS tags superior and advantageous to fluorescent dyes or quantum dots for use in complicated analyses.[18] Raman analysis results in short Raman scattering periods, compared with methods which may have higher scattering lifetimes, and decay as a result of lower photostability. This would make the SERS tags highly photostable. Further, SERS can be used as a non-invasive spectral analysis technique for *in vivo* analysis.[53,54]

The synthesis of the SERS tag begins with choosing the desired characteristics of the noble metal nanosubstrate. Single-particle substrate options can be explored, which include nanospheres, nanoshells, and nanorods. Each nanoparticle shape has their own advantages and disadvantages, but it is noteworthy that specialized shapes have a tendency to revert to the sphere shape over time as spheres are most stable. Nanoparticle cluster-based substrates are formed from aggregates of nanoparticles and have been developed for use as substrates for SERS tags. The aggregates generate strong electromagnetic fields and as a result have strong Raman scattering enhancing characteristics. Salt-induced aggregation is a common aggregation method for nanoparticles, among others. Gold and silver noble metals are most commonly used as SERS substrates. Gold offers high biocompatibility and easier controlled particle size distribution. In addition, a multitude of gold nanoparticle shapes and sizes have been reported in the literature with straightforward protocols. Silver offers a 10- to 100-fold higher SERS signal enhancement than gold but has poor biocompatibility and uncontrollable size distributions. Factors such as SERS signal enhancement and biocompatibility, among others, ought to be considered when choosing a noble metal substrate.[18,55]

Once the SERS substrate has been synthesized, the next step is to conjugate a Raman reporter molecule with the substrate. In order to achieve an optically enhanced Raman signal, the Raman reporter molecule must be either on or very close (ideally less

than 2 nm) to the surface of the SERS substrate. This is due to the distance-dependence of the electromagnetic field enhancement. Raman reporters are often materials containing nitrogen or sulfur due to their strong affinity for gold and silver. The interaction between the Raman reporter molecule and the noble metal substrate must be strong enough to avoid desorption during use in SERS or further modification steps, therefore materials of high affinity for each other are necessary.[18] Another consideration to make while choosing a Raman reporter molecule is the scattering cross section which results from the reporter, which should be large enough to produce a strong SERS signal. Ideally, the Raman spectrum of the Raman reporter molecule will be simple containing few peaks to avoid overlapping with the sample analyte.

Once the Raman reporter molecule is conjugated to the noble metal substrate, a surface coating is applied for protection. Interferences can occur in spectra without coating materials blocking the metal nanosubstrate, so to avoid these issues surface coating is applied. Interferences can come from the metal substrate adsorbing molecules in the sample environment, along with dissociation of Raman reporter molecules. Several coating types exist and can be considered for use depending on necessary considerations, for example biocompatibility. Some coating types include biomolecule coating, polymer coating, liposome coating, and silica coating. Biomolecule coatings must offer a high biocompatibility. Bovine serum albumin (BSA) is a commonly used biomolecule coating that forms a protective shell once mixed with the primary nanoparticle-Raman reporter SERS tag. Denatured BSA has also been used successfully as a biomolecule coating agent.[18]

Finally, the last step in SERS tag fabrication involves attaching capture agents. A multitude of targeting molecules exist which can be conjugated to the SERS tag. Some

examples of capture agents include antibodies, antigens, other small-molecule ligands, just to name a few. Once the SERS tag is complete, sample analysis applications can be explored. Several ionic and molecular detection methods can be coupled using SERS tags. There are options such as analyte-induced SERS tag aggregation and analyte-induced alteration of Raman reporter's signature that have been developed for ionic and biomolecular detection. The strategy of greatest interest in this project for detecting biomolecules is SERS-tag based immunoassay tests. This strategy started with antigen identification. These typically function as follows: antibodies exist immobilized on a substrate, and then antigen and antibodies that have been conjugated to SERS tags are added to the substrate. After washing steps to prevent non-specific binding, antigens can be identified via SERS analysis.[18] In this strategy, antigens could be interchanged with antibody identification. Further, SERS analysis has the potential for both qualitative and quantitative analysis of biomolecule samples. Protein detection has been achieved via a sandwich immunoassay format, a technique known as an ELISA sandwich assay, which allows for both qualitative and quantitative analysis. In the ELISA sandwich assay technique, an antibody is anchored to either an antigen which allows for capture of antibodies that are conjugated to SERS tags.[56] The sandwich technique can be seen in Figure 3 below. Finally, pathogen detection and live cell imaging are other bioanalysis applications where SERS tags serve as assets.[18]

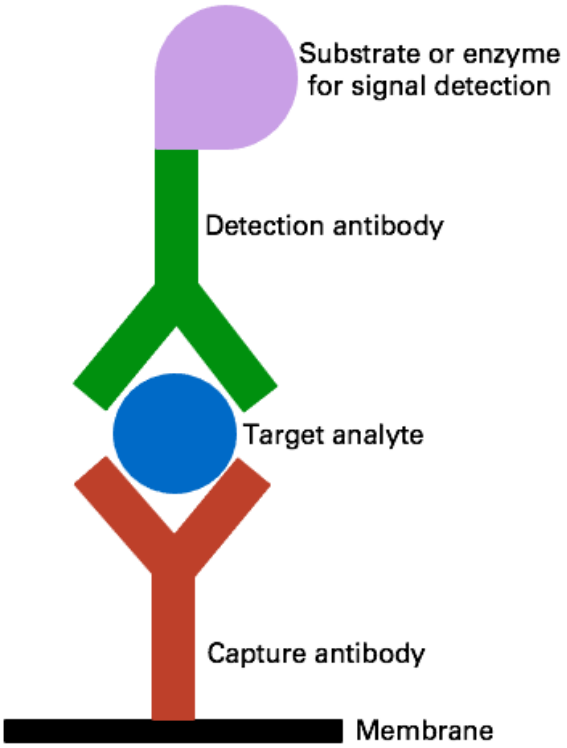

Figure 3. Sandwich immunoassay technique.

UV-Vis Spectroscopy

Ultraviolet-visible (UV-Vis) spectroscopy is a spectroscopic technique often used for quantitative determination of analytes. The UV-Vis spectral region typically comprises wavelengths from 200 to 800 nm. Both qualitative and quantitative information of a molecule can be obtained from UV-Vis spectroscopy, but due to an excellent adherence to Beer's law at low concentrations, quantitative analysis is the most useful application.[57] Most UV-vis spectrometers have similar instrumentation. The instrumentation typically includes a light source, a scanning monochromator, sample and reference cuvettes, a motor, mirrors, a detector, an amplifier, and a readout display or computer-based data analysis monitor.[58]

In absorption spectroscopy, measures of irradiance at frequencies before and after passing through the sample are measured and compared. Transmittance is measured, which is the ratio of the irradiance of the light beam emerging from the sample medium, to the irradiance of the incident beam. Absorbance is the negative logarithm of transmittance. The amount of absorption that occurs is linearly related to concentration, as observed in Beer's law. Also, absorption peaks can be used to identify compounds, most often by comparing unknown samples to known reference spectra.[57]

There are many useful applications of UV-Vis spectroscopy. Some of these include determining kinetics or rate constants of chemical reactions. An equilibrium constant of a reaction can also be calculated using UV-Vis spectroscopy.[59] Another relevant application of UV-Vis spectroscopy is determining the size and concentration of gold nanoparticle solutions. Further, spectra collected from UV-Vis of gold nanoparticles before and after modification can indicate whether they have been damaged or deformed.[60]

Scanning Electron Microscopy (SEM)

A scanning electron microscope (SEM) is an electron microscope that can capture images of sample with nanometer resolution. It functions by scanning the surface of a sample with an energetic beam of electrons. Once the electrons reach the sample, signals are produced and collected which give information about the surface composition and topography of the sample.[61] Signals are usually collected from the primary electrons, but additional signals are produced and can be collected from secondary electrons, back-scattered electrons, characteristic X-rays, absorbed current, and transmitted electrons. Given the cost of the equipment required to collect and analyze all of the signal types

produced, it is unlikely that a SEM would have the necessary hardware to detect all of the signal types.[62] Sample preparation for SEM can vary greatly based on the sample of interest. For example, the samples are typically small as they must fit inside the sample chamber. Additionally, some samples need to be coated in gold, copper, carbon, or other coating materials in order to increase the electrical conductivity or increase stability. Conductivity in samples is important as nonconductive samples may hoard charge from the electron beam, which may result in interference and inaccuracy of images. Most SEM samples are required to be dry because water or wetness can impact the images taken at the high vacuum.[63] SEM is an excellent tool for identifying the size and shape of nanoparticles, as well as identifying unknown samples by comparing them to known references. In addition, many SEM systems are also equipped with energy-dispersive x-ray spectrometers which allow for semi-trace elemental analysis of the sample using the scattered x-rays that are generated by the electron beam.

Lateral Flow Assay (LFA) Testing

Lateral flow assay (LFA) testing is used for the detection of target molecules in complex mixtures, including biological samples. LFA tests allow for point-of-care diagnosis and can be used in clinical laboratories and also in physician's offices and hospitals. They allow for detection of antibodies, antigens, along with products of gene amplification. Several biological samples can be used in LFA testing, including urine, saliva, sweat, blood, among others. There are various types LFA tests which differ based on the type of target molecule. These tests include nucleic acid lateral flow assay tests and

lateral flow immunoassay tests.[64] A breakdown of the lateral flow assay test types can be seen in Figure 4.

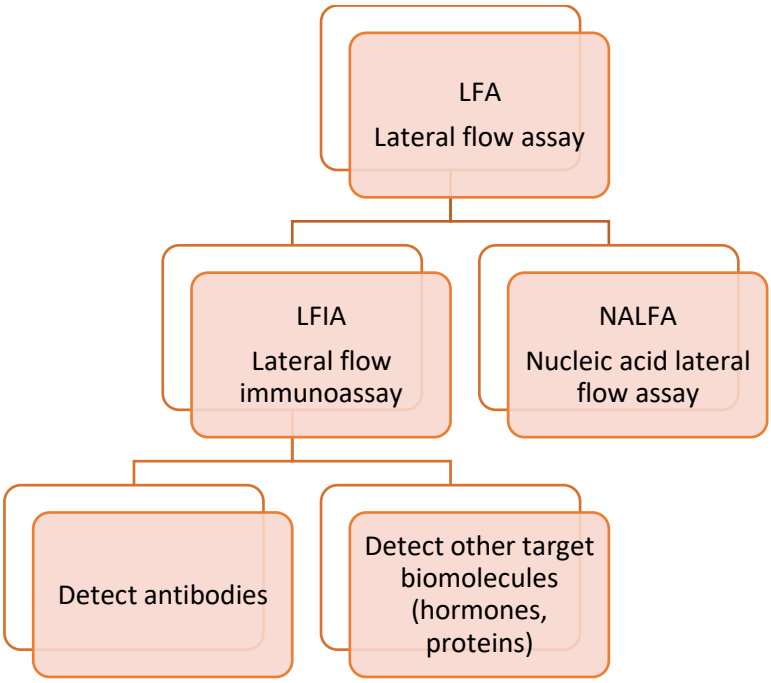

Figure 4. Common lateral flow assay test types.[64]

Nucleic acid lateral flow assay tests detect nucleic acids. Lateral flow immunoassay tests antibodies. LFA tests are composed of a sample pad, conjugate release pad, membrane, and absorbent pad. The sample pad is used to evenly distribute the sample and direct it in the direction of the conjugate bad. The conjugate pad holds detector particles. The membrane holds immobilized antibodies and both test and control lines. The absorbent pulls the liquid sample through the test via capillary forces and collects the processed sample liquid.[64] The components and arrangement of LFA tests can be seen in Figure 5.

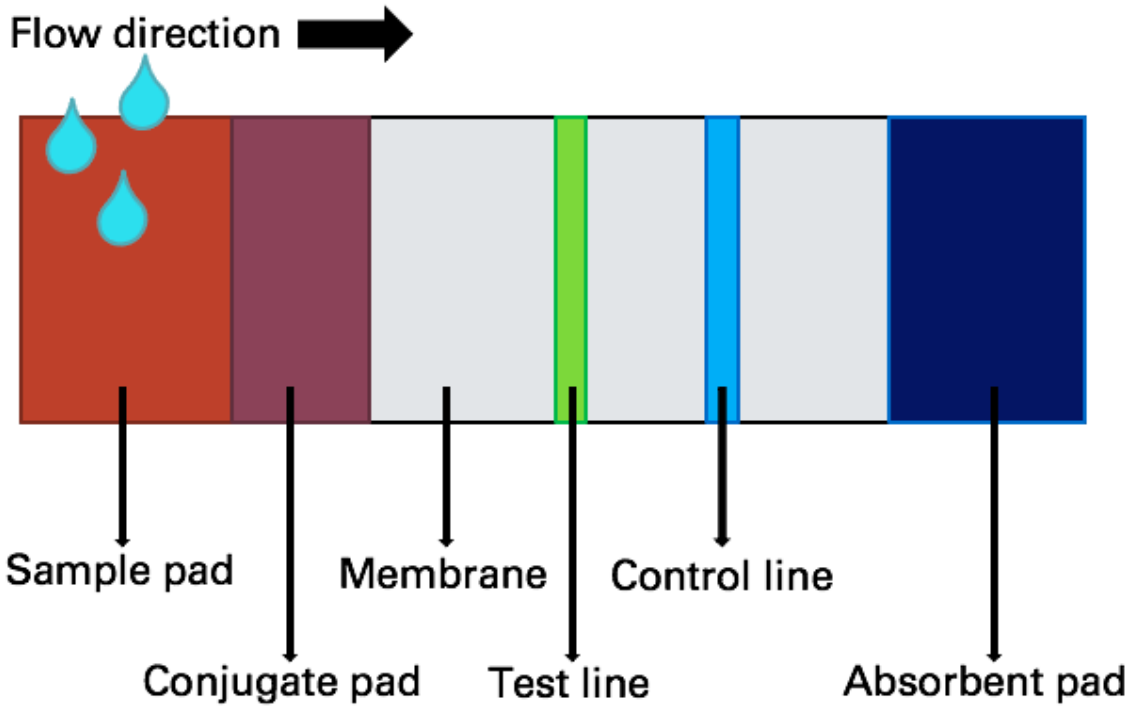

Figure 5. The components of typical LFIA tests and their alignment in test system. The components lie on a backing card or other test cartridge backing.

LFIA tests typically offer low development costs and production costs. However, they tend to have low sensitivity and selectivity.[64,65] Their low sensitivity and selectivity is why LFIA tests coupled with SERS are ideal; the SERS aspect increases sensitivity and selectivity.

Methods and Materials

Reagents and Materials Used: Table 2 lists the materials and reagents used in this thesis research. All reagents were used as received without further purification. All solutions were prepared using Millipore water (> 18.2 MΩ cm).

Table 2. Materials and apparatuses used.

Material	Material Description	Manufacturer	Location
Nitric acid	67-70% HNO_3	Fisher Scientific	Canada
Hydrochloric acid	34-37% HCl	Avantor	USA
Sodium bicarbonate	99% purity	Sigma Aldrich	USA
pH paper	N/A	Fisher Scientific	USA
Sodium citrate	>99% purity	ACP Chemicals	Montreal, Québec
Chloroauric acid	>99% purity	Stream Chemicals	Newburyport, MA, USA
Ultrapure water	>99% purity	N/A	Nova Scotia, Canada
PYOT	97% purity	Sigma Aldrich	India
Cellulose filter paper	3.0 mm diameter	Whatman	Maidstone, England
Nitrocellulose	47 mm diameter, 0.46 μm pore size	Whatman	Maidstone, England
Glass slides	N/A	Sigma Aldrich	USA
Carbon electrode	N/A	Pine Research	USA
Kimwipes	N/A	Kimberly-Clark	USA
Protein A	N/A	Sigma Aldrich	Israel
Bovine serum albumin	96-99% albumin	Sigma Aldrich	St. Louis, MO
Immunoglobulin G	N/A	Sigma Aldrich	St. Louis, MO
Eppendorf tube	Type brand	Sigma Aldrich	St. Louis, MO
Silica wafer	N/A	Ted Pella	USA
Double-sided carbon tape	N/A	Nisshin Em. Co. Ltd	Japan
Acetone	N/A	Fisher Scientific	USA
Petri dish	N/A	Fisher Scientific	USA
Micropipette	Various volumes	VWR	Hannover, Germany

Methods: Sample Preparation

AuNP Synthesis Procedure

A method for the kinetically controlled seeded growth synthesis of citrate-stabilized gold nanoparticles was developed by Bastús et al. and is the synthetic method used in this study. In this method, the gold nanoparticle "seeds" are first synthesized. Next, the gold nanoparticles are grown via a seeded-growth method which allows for control over particle diameter. Briefly, a 2.2 mM solution of sodium citrate was prepared using ultrapure water. The solution (150 mL) was heated to boiling in a flask. A reflux condenser was used to avoid evaporation of the solvent. Once the solution reached boiling, 1 mL of 25 mM $HAuCl_4$ was quickly injected into the flask. After boiling for approximately 10 minutes, the solution changed from yellow, to blue, to pink. The particles that result from the aforementioned steps are gold nanoparticle seeds coated in citrate ions. Next, the gold nanoparticles increase in diameter via a seeded growth process. The solution of gold seeds in the flask was cooled from boiling to 90°C. Once the temperature reached 90°C, 1 mL of 25 mM $HauCl_4$ was injected into the three-necked round-bottomed flask. At this point, the solution was left under reflux for 30 minutes and the temperature was kept at 90°C. This process was repeated twice. Next, the solution underwent a two-fold dilution. This was done by extracting 55 mL of the solution and combining it with 53 mL of ultrapure water and 2 mL of 60 mM sodium citrate. This solution was then used as the seed solution for further dilutions, and the process was repeated again. Five dilutions were carried out in order to produce varied gold nanoparticle sizes. Several gold nanoparticle sizes allow for testing of each size, which allow for size optimization in future work. This method developed by Bastús et al. allows for careful control of size and shape of gold nanoparticles.

5-(4-Pyridyl)-1,3,4-oxadiazole-2-thiol (PYOT) solution

PYOT is used as the Raman reporter in the development of the SERS tags explored in this thesis work. First, the glassware was soaked in a concentrated sulfuric acid bath overnight for thorough cleaning, then rinsed excessively with ultrapure water. The flask was left upside down to rinse and dry. Solid PYOT was weighed on the analytical balance to 0.0035 g to make the 0.8 mM initial stock PYOT solution. The solid PYOT was transferred to the volumetric flask from the weighing paper which was rinsed with water to ensure all PYOT was transferred. Next, the flask was filled with ultrapure water, but not to the line. The flask was then placed in a 250 mL beaker containing 100 mL of water which was heated close to boiling on a hotplate. After approximately 20 minutes, the solid PYOT was fully dissolved. The solution was then filled to the line and stored in the fridge. For use in the conjugation process, the solution was diluted to 0.12 mM concentration.

SERS Sample Preparation

Gold nanoparticle suspensions were analyzed using SERS. SERS analysis requires a Raman reporter molecule to be associated with the nanoparticle sample in order to enhance the signal. The Raman reporter molecule used in this study was 5-(4-Pyridyl)-1,3,4-oxadiazole-2-thiol (PYOT). For the SERS analysis, 5 μL of gold nanoparticle solution was placed onto the substrate and left to dry. This was repeated twice, for a total of 15 μL of gold nanoparticle solution. Next, 5 μL of PYOT was deposited onto the dried gold colloid and left to dry. A control sample was made without gold nanoparticle solution and with PYOT exclusively. Finally, a blank sample was included which was the substrate on its own (no PYOT). The aforementioned SERS sample preparation method was used

with several different substrates. These included glass slides, carbon electrodes, cellulose-based filter paper, and nitrocellulose membrane filters.

Further, SERS analysis was conducted using the gold nanoparticles after the conjugation process (addition of PYOT, protein A and bovine serum albumin). The SERS analysis was completed on the modified particles before and after centrifugation. In each case, 5 μL of solution was deposited on the nitrocellulose substrate and allowed to dry before SERS analysis.

UV-Vis Sample Preparation

In order to achieve a readable UV-Vis spectrum of gold nanoparticle samples, the suspensions needed to be diluted with ultrapure water. First, the glass UV-Vis cuvette was emptied and rinsed with the gold nanoparticle suspension. Once rinsed, the cuvette was filled with the appropriate amount of suspension in order to achieve the desired dilution factor. The suspension was filled near the top of the cuvette with ultrapure water, and in future scans the cuvette was filled with the same volume for the sake of consistency. The desired dilution factors in this study were three and six. It was ensured that the level of the blank and sample was high enough, so the light beam passed through the sample. It was also ensured that there were no air bubbles in the sample.

SEM Sample Preparation

For gold nanoparticle SEM analysis, silicon wafers were used as the substrate. These silicon wafers are atomically flat, and thus a preferred substrate for imaging of

particles which are close to the spatial resolution limit of the instrument. The aluminum SEM peg was cleaned with acetone and placed in the sample holder. A piece of double-sided carbon tape covered the top of the peg. A silicon wafer was placed on the carbon tape and the corners were pressed down, with the shiny side facing up. Finally, 5 μL of gold nanoparticle sample was placed on the silica wafer and allowed to dry. This procedure was repeated for all gold nanoparticle size samples. Tweezers and gloves were used throughout to handle sample materials. After sample preparation was done in the lab, further sample preparation was completed in the SEM workspace. Several of the samples were coated in gold and carbon to improve the image quality.

Conjugation Process

Gold nanoparticles, PYOT, Protein A, and BSA solutions are required for the conjugation process. This process is an adaptation of a method reported by Brosseau et al. for the preparation of SERS tags for point-of-care vertical flow assay technology.[33] To start, the first step in the conjugation process involves adding 990 μL of gold nanoparticle suspension to an Eppendorf tube using a micropipette. Next, 10 μL of 1.0 mg mL^{-1} Protein A solution is added to the Eppendorf tube and aspirated with a micropipette. The tube is then taped to a piece of paper and rocked on a rocker for 30 minutes at a medium to high setting. Visual observations of colours is important before and after rocking the solution, since colour changes (i.e. red to purple or grey) can indicate particle instability during the process. Once the solution has been rocked, 320 μL of 0.12 mM PYOT is added to the tube and aspirated with a micropipette. Then, 1 μL of 1% bovine serum albumin is added to the tube and aspirated with a pipette. The tube is then rocked for another 30 minutes. After 30

minutes, the tube needs to be centrifuged for 30 minutes. In this thesis work larger nanoparticles were used, so 6000 to 8000 rpm speeds were used as settings while using the centrifuge. Careful attention is to be taken to ensure the centrifuge is balanced. The supernatant was removed using a micropipette, and a pellet remained in the tube. Samples were taken from the tube at various stages thorough the conjugation process for SERS and SEM analysis.

IgG Activity Test Preparation

The activity of immunoglobulin G (IgG) was verified using a new method. Protein A was used in the conjugation process as a way to anchor IgG to the SERS tag molecule to allow for is functionality. Protein A has a high affinity for IgG and has a high selectivity for target molecules, which makes it an optimal choice for use in serology testing. Recall, IgG is a long-lasting SARS-CoV-2 antibody present post-infection, so its use as a detection antibody in serology testing is sensible. In the conjugation process, once Protein A was conjugated to the gold nanoparticles, the IgG activity was tested. This was done by comparing the result of conjugated Protein A-nanoparticles mixed with IgG with conjugated Protein A-nanoparticles mixed with human saliva, known to contain active IgG protein. A control test was also completed which contained conjugated Protein A-nanoparticles alone. The test platforms used were modifications of commercially available test cartridges for vertical flow assays. The active test membrane from the test cartridge was removed and replaced with cellulose and nitrocellulose substrates prepared in the laboratory. Then the 5 μL of IgG solution and 5 μL of saliva were deposited on their respective test substrates. They were immediately followed by 5 μL of the Protein A

conjugated-gold nanoparticles, and then rinsed with 10 to 20 μL of ultrapure water. The test components can be seen below in Figure 6. The tests were also run with diluted conjugated solutions with dilution factors of 3 and 6. SERS and SEM analysis were completed for the modified test cartridges.

Figure 6. IgG activity test components. The components include a test cartridge backing, an absorbent pad, nitrocellulose membrane, and test cartridge cover with opening for blotting sample.

SERS Analysis

An Advantage 785 benchtop Raman spectrometer was used for SERS analysis in this thesis work. This spectrometer uses a 785 nm laser and is equipped with an air-cooled CCD. For analysis of the substrates explored in this work, the right-angle optics attachment was used. It was essential that all jewelry was removed before use to avoid specular reflection. Laser safety glasses were also required to be worn during use. NuSpec software was used for SERS analysis. In order to ensure the detector was able to draw in cool air to cool the detector an oscillating fan was directed onto the back of the instrument. In order to verify the laser was focused on the sample, the integration time was set to 1 second and the power was set to low. A continuous spectrum is displayed, and the laser glasses were briefly removed to verify the position of the sample and optimize the laser focus. The continuous signal was then aborted, and the integration time was changed to acquire the desired spectra.

For all SERS samples, 10 spots on the test sample were analysed on the same substrate. The average signal of the 10 plots were taken and reported. The integration time remained 30 seconds for every experiment run throughout the project. SERS analysis was completed at each dilution of gold nanoparticle solution. The different dilutions correspond to various nanoparticle sizes, and SERS was used to determine the optimal nanoparticle size with the PYOT Raman reporter. The optimal size determined via SERS analysis was used for future work, including the conjugation process. In general, nanoparticles with diameter between 40 and 100 nm work best for SERS analysis and biomolecular conjugation processes. SERS analysis was also complete at various steps throughout the conjugation process.

UV-Vis Analysis

An Agilent Cary 60 Spectrophotometer was used to obtain UV-Vis spectra. The Cary WinUV online software was used for data interpretation. The range was set for 200 to 800 nm, which is an optimal range when analyzing nanoparticles. Baseline correction is required, and water was used at the blank solution. Once the blank spectrum has been collected, a zero-transmittance spectrum is taken as another correction. Once these spectra have been obtained, the sample can be run and the spectrum of interest may be obtained.

Chemical Cleaning Methods

Aqua Regia Preparation

Aqua Regia is a cleaning solution containing HCl and HNO_3 in a 3:1 ratio. Aqua regia was used to clean the three-necked round-bottomed flasks, along with other glassware, that came in contact with gold. For the purpose of the 250 mL three-necked round-bottomed flasks, 15 mL of HCl and 5 mL of HNO_3 were used to make the aqua regia solution. The 15 mL of HCl was first added to the three-necked round-bottomed flask, followed by the 5 mL HNO_3. It is always required that the HCl be added first, followed by the HNO_3. The mixture was stirred to reach all of the flask to ensure adequate cleaning. Once finished, the solution was transferred to a beaker and neutralized with $NaHCO_3$. Once the pH was verified to be neutral with pH paper, the solution could be diluted with water and disposed of down the drain. Proper precautions, including a face shield, rubber apron, and rubber gloves were used as PPE, along with typical laboratory PPE.

Acid Bath Procedure

An acid bath comprised of concentrated sulfuric acid was used to thoroughly clean all glassware used in this research. The glassware is rinsed, and labels removed before being added to the acid bath. Ideally, glassware remains in the acid bath for 24 hours, but as little as 1 hour may be adequate. Teflon-coated tongs are used to add and remove glassware from the acid bath, and additional personal protective equipment (PPE) are used, including a rubber apron and rubber gloves. Once removed, the glassware needs to be thoroughly rinsed 30 times with Millipore water.

Experimental Results

AuNP Characterization

UV-Vis Spectroscopy

The gold nanoparticle solutions were characterized using various methods, including SEM and UV-Vis spectroscopy. SEM and UV-Vis analysis provide valuable information concerning the size and shape of the synthesized nanoparticles. A seeded-growth method was used for the purpose of synthesizing gold nanoparticles of various sizes. Once the particles of varied size are synthesized, the particles of different size may be tested to determine the optimal size for future work in the study. The results of the UV-Vis analysis are seen in Figure 7. The differences in maximum absorption wavelength indicate the gold nanoparticles vary in size. Particles exhibiting higher maximum absorption wavelength values are shifted towards the red visible wavelength spectrum. In addition, polydispersity of the sample results in broader peaks, and so a larger FWHM value typically indicates a larger distribution of particle sizes in the sample.

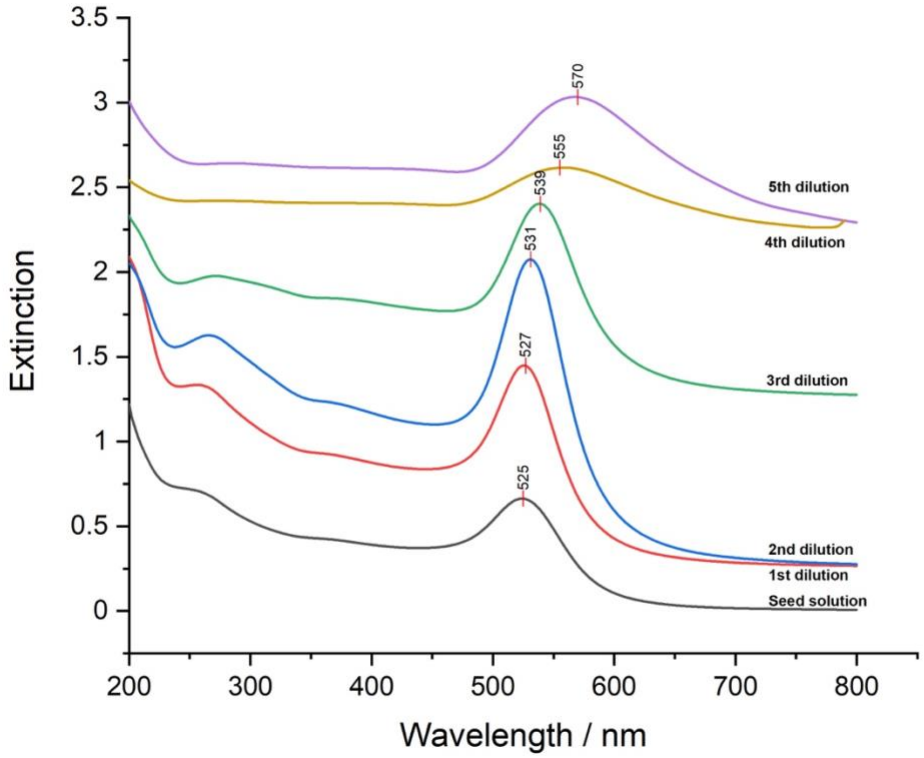

Figure 7. A UV-Vis extinction spectrum of bare diluted gold nanoparticle solutions at varied stages in the seeded-growth synthesis.

The maximum absorption wavelengths vary from approximately 525 to 570 nm lying in the visible light spectrum. The maximum absorption wavelengths are consistent with spherical gold nanoparticles. The various dilutions appear different in colour, which is explained by the differences in maximum absorption wavelengths. The suspensions containing smaller particles appear dark reddish purple, whereas the solutions containing larger particles appear more reddish orange. A sample of the gold nanoparticle solutions can be seen in Figure 8.

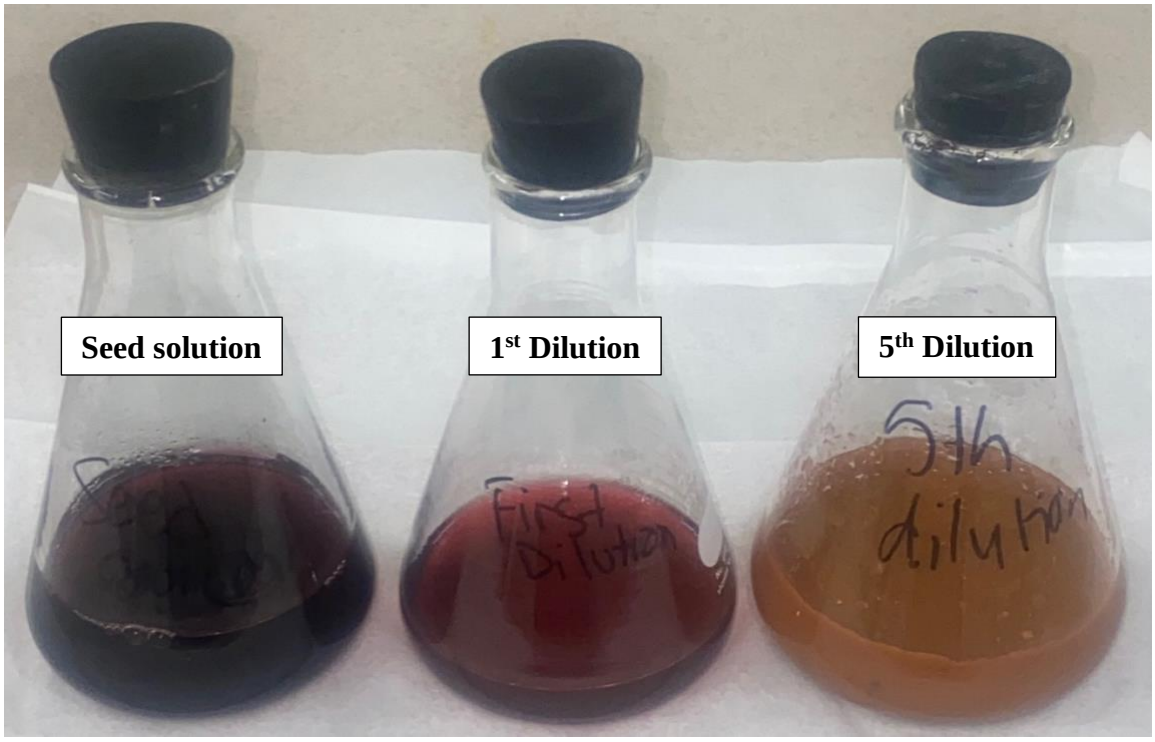

Figure 8. The seed solution, first dilution, and fifth dilutions of spherical, bare gold nanoparticle solutions.

SEM

Once the AuNPs were synthesized, they required characterization by SEM in order to analyze their size and morphology. Figure 9 includes SEM images acquired for the AuNPs, prior to conjugation steps.

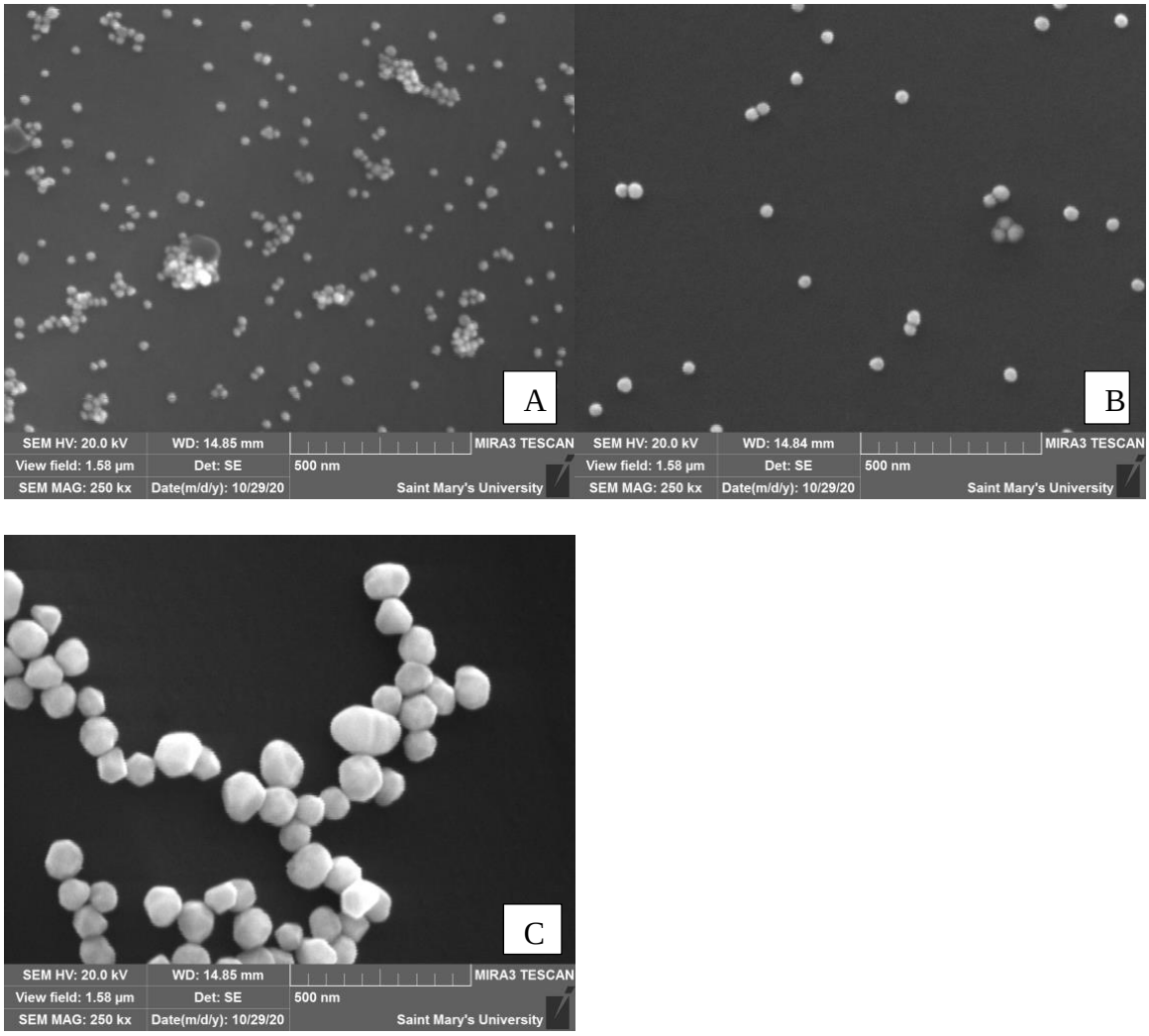

Figure 9. SEM images of the AuNPs at various dilutions using the same parameters; 150 kx magnification and 20 kV beam. (A) Seed solution, (B) first dilution, and (C) fifth dilution.

Data analysis was performed on the SEM images using the software Image J. The data obtained using image J can be found in Table 3. The SEM images were analyzed with Image J to determine the average size of the AuNPs, specifically their diameter. The data generated from Image J is consistent with the particle diameter data acquired directly from the SEM software analysis. Determining the size of the AuNPs was crucial in this project because the various sizes are to be analyzed via SERS using PYOT as the Raman reporter in order to determine which size gives rise to the optimal SERS signal intensity.

Table 3. The AuNP average diameter sizes in nanometers based on 10 measurements along with the standard deviation.

Sample	Average Diameter (nm)	Standard Deviation (nm)
Seed suspension	18.7	2.2
First dilution	28.1	2.7
Second dilution	42.8	2.6
Third dilution	56.7	2.7
Fourth dilution	74.1	2.9
Fifth dilution	88.7	2.9

The AuNP diameters found of the varied dilutions seen in Table 3 increase from 18.7 to 88.7 nanometers. This is a promising result, as it is hypothesized that larger nanoparticles will be optimal for use in the SERS tag being engineered.

IgG Test

The activity of IgG in an IgG solution was verified using modified Medmira test cartridges. The tests had originally been used for detecting target molecules such as hepatitis C virus, human papillomavirus, human immunodeficiency virus, among others. Visual analysis was the first method of detection possible for these tests. Following the visual analysis, the tests were analysed using Raman spectroscopy. The sample pads containing target molecules were removed and discarded from the test cartridges and were replaced with cellulose or nitrocellulose membranes which lacked target analytes at this stage. At this stage it was possible to obtain novel results from the tests. The starting point for visual analysis of the modified test cartridges is a bare sample pad.

Since the IgG solutions have a shelf life where activity is optimal, before continuing with the conjugation process it was necessary to verify adequate activity remained in the IgG solution which is required for the SERS tag to be functional. To review, the conjugated particle being synthesized is composed of AuNPs which are conjugated to Protein A, followed by the addition of PYOT and finally BSA. The protein A on the AuNP surface has an affinity for IgG which is meant to be trapped by the fixed antibody on the test site of the LFIA test. The IgG must be active, or else the test line will not appear, and the SERS tag particle will not be functional.

Figure 10 shows three of the modified cartridges with a cellulose substrate. The tests are composed of an absorbent pad, a substrate, and test cartridge backing and cover with an opening to allow for sample blotting. The sample analyte is blotted on the membrane and analysis. Their results can be read visually on the test sample pads. Additionally, the tests can be analyzed using SERS and SEM to verify results and obtain further information. SERS and SEM results can be seen in Figure 11 for further analysis of

the IgG tests. The coffee ring effect must be understood in interpreting the results visually. Briefly, the coffee ring effect describes the mechanism by which a pattern forms when solutions containing particles evaporate. The coffee ring pattern of the particles deposited result from a form of capillary flow. A contact line of the deposited liquid dries, and liquid flows from the interior of the drop to the contact line, to replenish the evaporated liquid. The flow of liquid outwards carries the particles to the edge of the drop, which creates the coffee ring effect. Gold nanoparticles tend to aggregate, so they strongly experience the coffee ring effect. This effect can be slightly observed in the IgG test cartridges seen in Figure 10.

Figure 10. The gold nanoparticle-Protein A conjugated particle tested with IgG solution, human saliva, and a control containing the gold nanoparticle-Protein A conjugated particle alone. The test substrate is a cellulose filter paper. A faint ring can be seen in the IgG and human saliva test, and not in the control test, indicating the IgG is active.

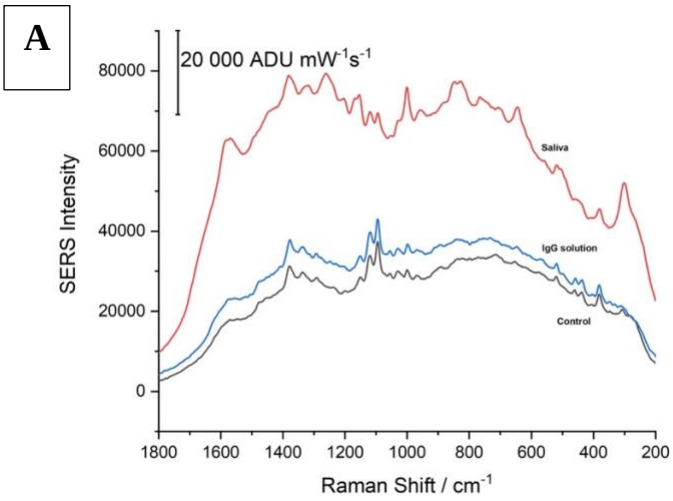

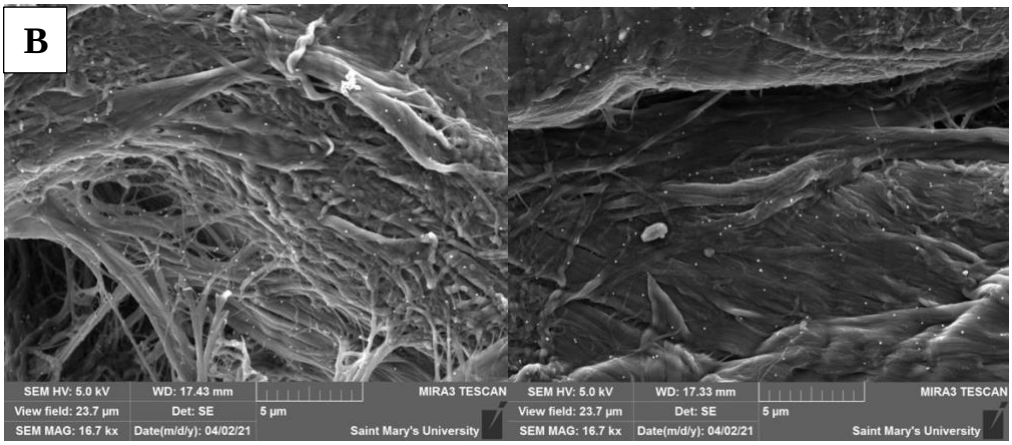

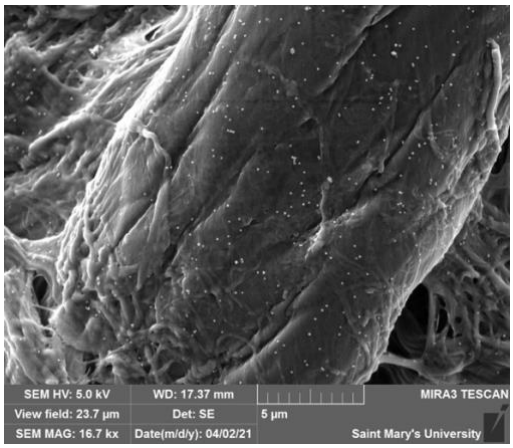

Figure 11. (a) SERS results of IgG activity test using cellulose substrate at 55.9 mW laser power and 30 second acquisition time. The saliva, IgG solution, and control solutions are included, and were not diluted in this analysis (b) SEM images of the IgG activity test using a cellulose substrate from the parameters 10 kx magnification and 5.0 kV beam. The images include the control test, the IgG solution test, and the saliva test, respectively.

On the modified Medmira tests for IgG activity, visually, it appears that the IgG has bound to the Protein A-NP conjugated SERS tag when the coffee ring is apparent and intense, in comparison to the control which lacks IgG. The control lines appear more faintly. A slight line may still appear in the control line, because the Protein A-NP conjugated particle may experience the coffee ring effect on the substrate without the active associated IgG. The coffee ring effect does not apply exclusively to metal nanoparticles conjugated with proteins and antibodies, as other particles may aggregate and stick to the sample pad via capillary forces. The results of the SERS analysis of the test seen in Figure 10 indicate the IgG solution is still active, which is additional support in the case that visual interpretation is not possible or is inconclusive. The intensity of the SERS signal is greater on the IgG solution test spot compared to the control spot and is less intense than the saliva control assumed to contain relatively high concentrations of active IgG. The results are promising and indicate the IgG solution can be used in the conjugation process with little risk of inactivity. Tests were done with concentrated gold nanoparticle solutions, along with diluted solutions to verify the coffee ring effect does not result from overly concentrated solutions staining the test substrate.

The test cartridges were also modified to contain a nitrocellulose sample pad. The IgG activity tests using nitrocellulose as a substrate gave different results, as can be seen in Figure 12. This substrate was tested along with cellulose as nitrocellulose is the substrate used in SERS analysis and in typical LFIA testing.

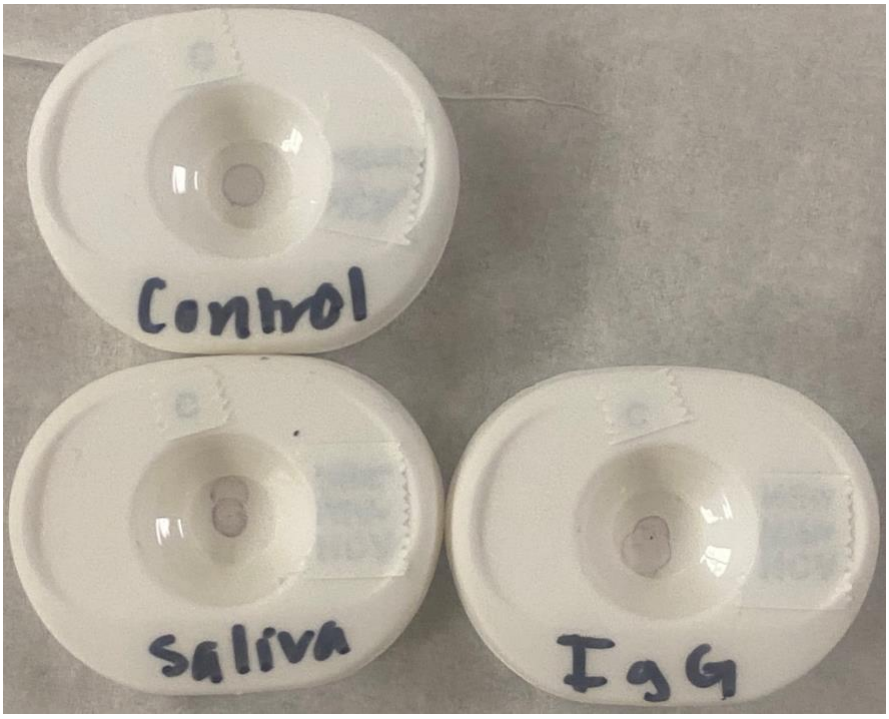

Figure 12. Results of IgG activity tests using nitrocellulose as a substrate.

Visually, it was much more difficult to interpret a difference between test and control lines. This is because nitrocellulose is less absorbent than cellulose filter paper. As a result, these tests relied more heavily on SERS and SEM analysis, which can be seen is Figure 13.

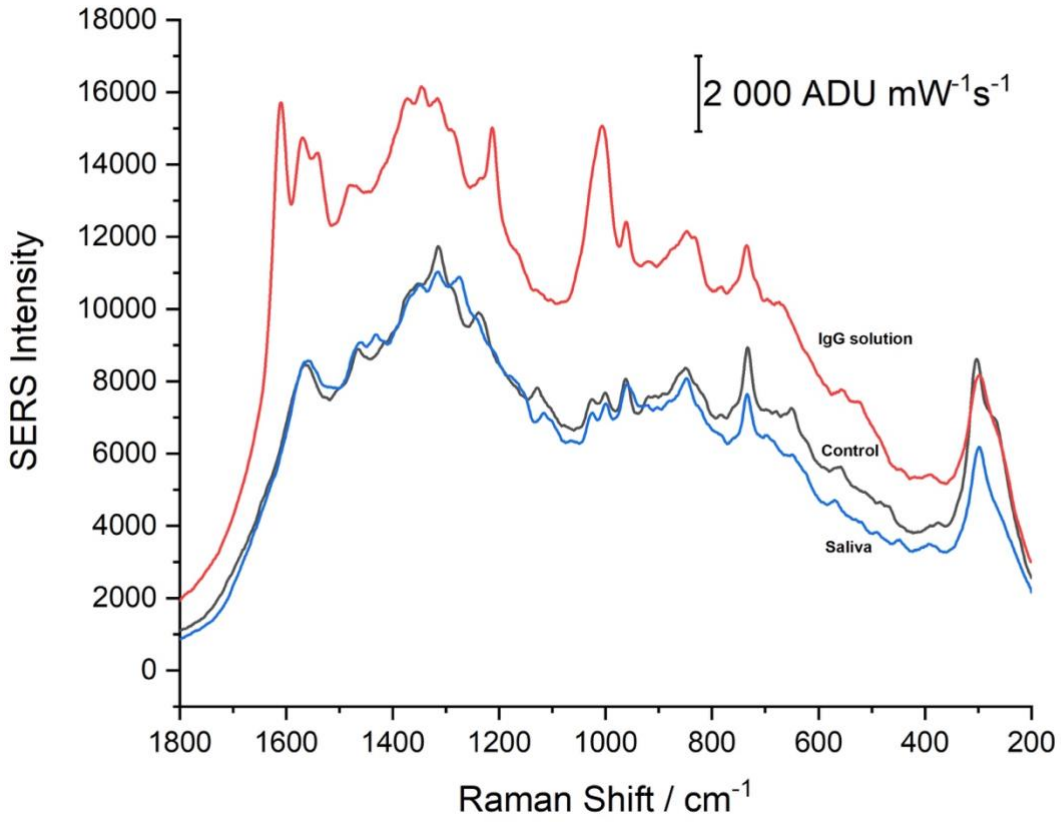

Figure 13. SERS results of IgG activity test using nitrocellulose substrate at 10.6 mW power and 30 second acquisition time. The saliva, IgG solution, and control solutions are included, and were not diluted in this analysis.

The SERS results are promising indicators that the IgG solution tested contains active IgG. The SERS intensity is significantly greater in the IgG test compared to the control solution. Although the SERS results from the saliva test are less intense than the IgG test, it is not necessarily suggestive of an abnormal or inconclusive IgG activity result. A lower concentration of IgG could exist in the saliva sample and explain the difference in SERS intensity. Also, saliva would contain other biomolecules other than IgG, which could impact SERS results.

Initial SERS Tag Analysis

Throughout the SERS tag engineering process, several analyses needed to be taken at various stages. After the synthesized AuNPs were characterized to determine their size and morphology, they could move forward with the engineering process. The AuNPs of various diameters were coated with the PYOT Raman reporter molecule as preparation for initial SERS analysis. This analysis is required in order to determine the optimal particle size to be used for future conjugation steps in the SERS tag analysis process. The optimal particle size would offer strong SERS signal with little variability and few to no spectral interferences

Substrates are required while conducting SERS analysis to hold the sample being tested. These may include regular filter paper or glass material slides as substrates, among many other materials. The substrates should offer very weak SERS signals and provide very few interferences. First, glass slides were used as the SERS substrate. Some of the SERS results obtained of the AuNP conjugated with PYOT on glass slides may be found in Figure 14.

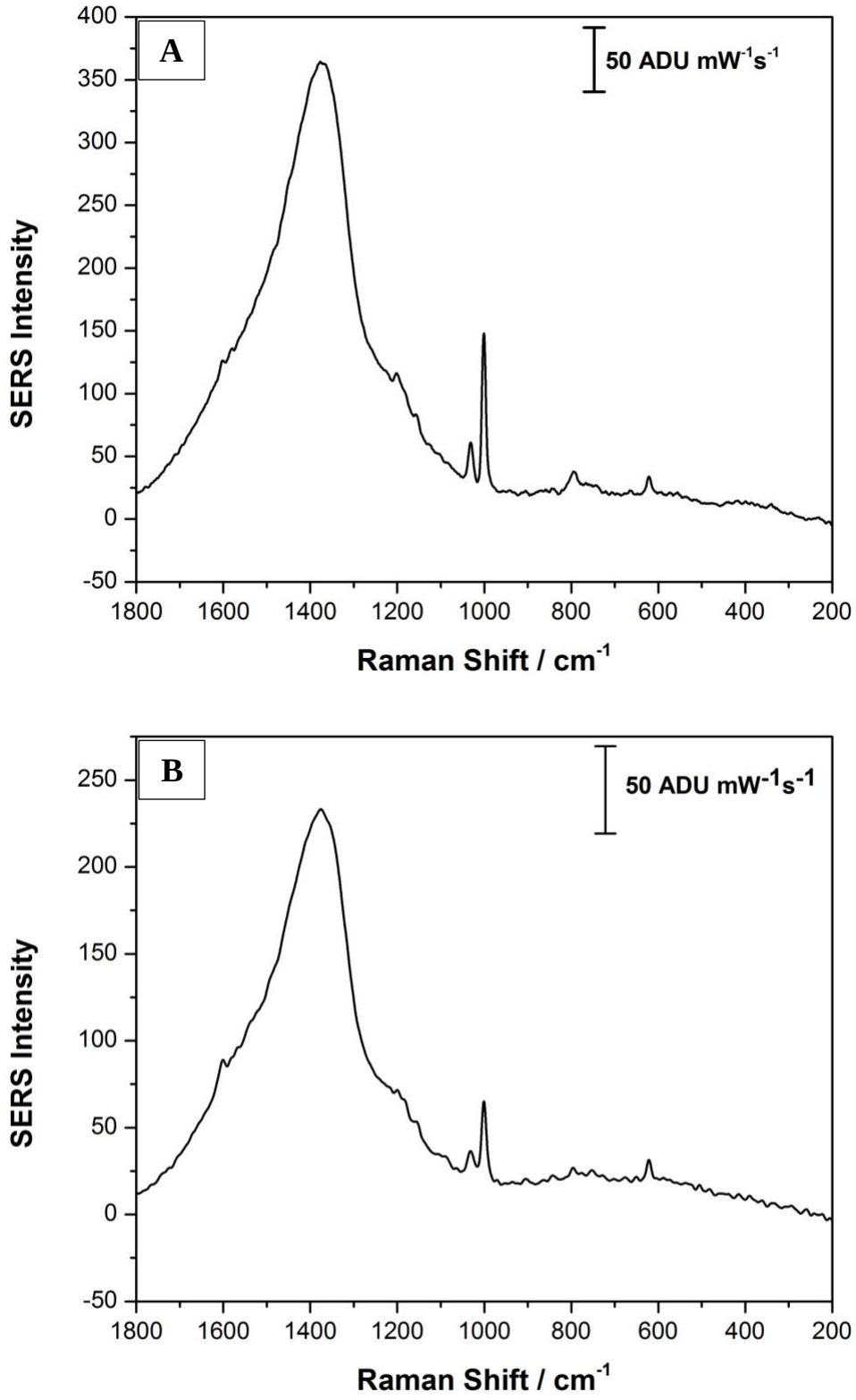

Figure 14. SERS spectra collected from (A) 3 coatings and (B) 1 coating of 5 μL AuNP seed solution covered with 5 μL of PYOT at a 2.93 mW laser power and 30 second acquisition time.

The glass substrate proved to be an unsatisfactory SERS substrate in the analyses. As can be seen in Figure 14, there is a large broad peak near 1400 cm^{-1}. This peak is a glass interference peak and does not allow for interpretation of the AuNP conjugated PYOT peaks. The setback due to the glass interference, although minor, slightly delayed progress. Upon the realization of the glass interference, new samples were prepared to acquire SERS signals using carbon electrodes as substrates. The carbon electrode substrates were only briefly explored, and results can be seen in Figure 15.

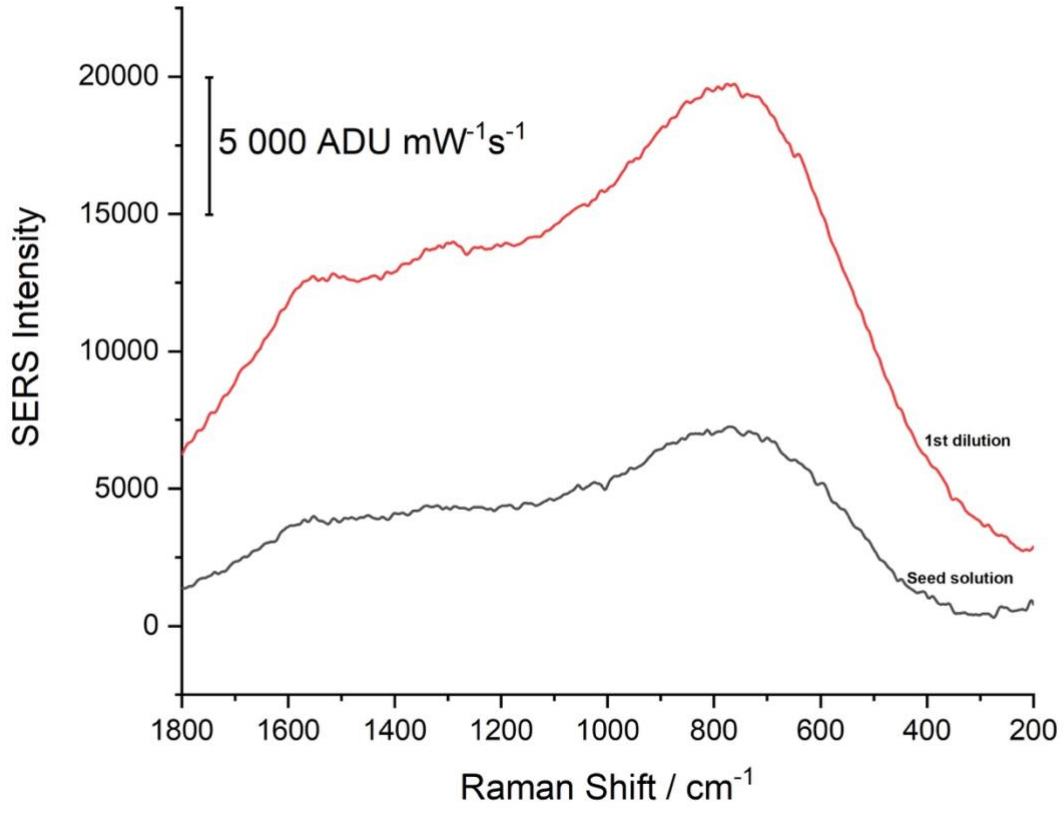

Figure 15. SERS analysis of AuNP coated with PYOT on carbon electrode substrate at 22.3 mW laser power and 30 second acquisition time.

Unlike the glass slide, the carbon electrode substrate did not demonstrate the interference found at 1400 cm^{-1}. No PYOT signal was observed using the carbon substrate, because the AuNP sample layer was too thin and the Raman spectra obtained is for carbon, with fluorescence interferences. The carbon electrode was not used as a SERS substrate for the duration of the research project, so the SERS analysis were not reattempted for improved spectral results. Given that nitrocellulose is the membrane material most often used in LFIA testing, it acted as the optimal material for use as the SERS substrate for future SERS analysis and other future work in the conjugation process. Nitrocellulose is ideal and would introduce less variables than alternative substrates. Nitrocellulose can be costly, and initially made it prohibitive for use as the substrate. Therefore, regular cellulose filter paper was used to continue with the SERS analysis. The SERS results obtained using a cellulose substrate may be found in Annex A. Once the nitrocellulose was obtained, it was used as the SERS substrate for all analysis. The SERS results obtained using a nitrocellulose substrate of the AuNP coated with PYOT may be found in Annex B. The SERS analysis of the 4^{th} dilution of the AuNP solution coated with PYOT may be seen in Figure 16.

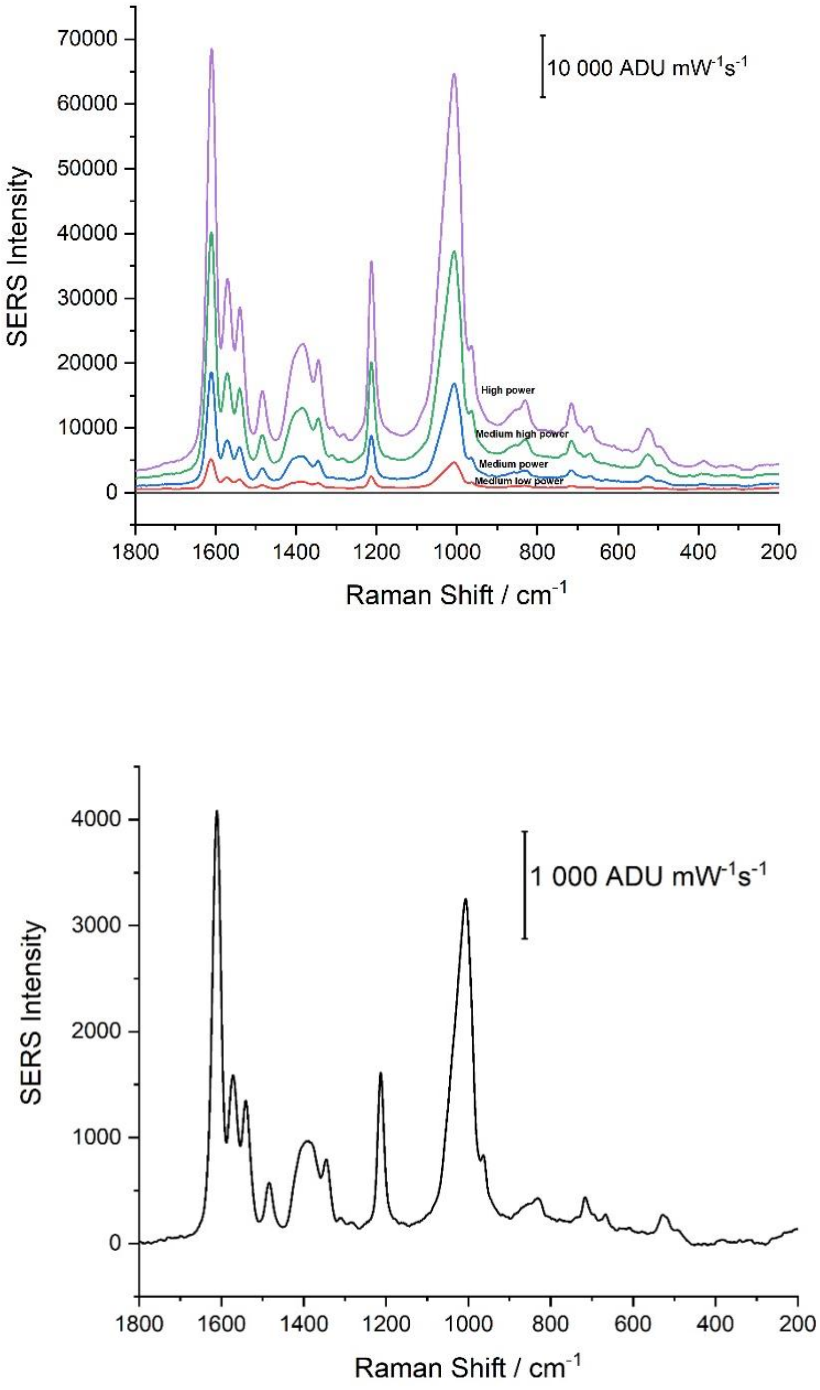

Figure 16. SERS analysis of the 4th dilution of three 5 μL AuNP solution coated with 5 μL PYOT with (a) demonstrating an offset of 2.93, 10.6, 22.3, 46.5, 55.9 mW laser powers and (b) demonstrating 10 sample spots averaged at 10.6 mW laser power.

The optimal AuNP size was determined to be from the 4th dilution. This was based on the spectra obtained which appeared generally free from substrate or other interferences. Further, the reproducibility was considered when choosing this as the optimal particle size. Therefore, the SERS tag engineering including the conjugation process was completed with the 74.1 ± 2.9 nm particle diameter size from the 4th dilution.

AuNP size analysis

The size and morphology of nanoparticles strongly impacts the characteristics that result when they are used in various applications. Since the implications of size and morphology are so significant, they are worth being studied further. Also, a significant portion of the optimization processes that take place in this project concerned AuNP size and its relation to SERS analysis. Therefore, the direct relationship between nanoparticle diameter and SERS intensity was studied and can be found in Figure 17 below.

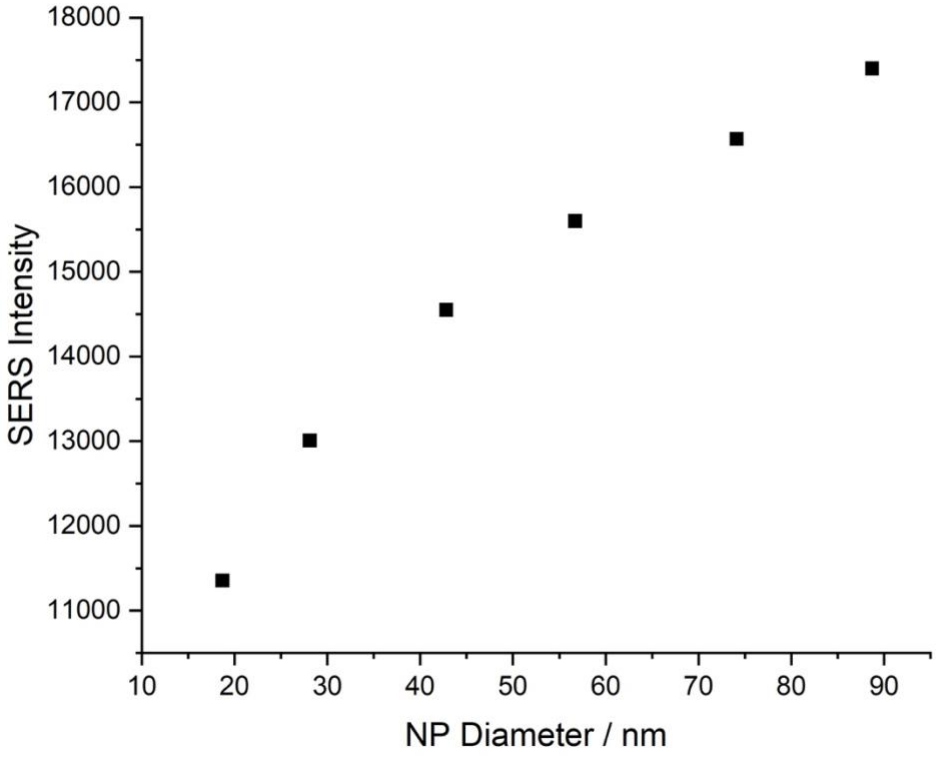

Figure 17. The relationship between SERS intensity and AuNP diameter based on various AuNP dilution sizes and their SERS intensity at a 1600 cm^{-1} PYOT peak at 10.6 mW laser power.

As can be seen in Figure 17, the SERS intensity appears to relate directly to AuNP size in diameter. The relationship appears to be linear, at least for the diameter range of 18.7 to 88.7 nm. The relationship between SERS intensity and larger AuNP diameters was not explored, however it is reasonable to expect that eventually the relationship would level off and the SERS intensity would increase less with size increase after a point. The nanoparticles could become too large for practical use. Therefore, the particle size range obtained in this study is satisfactory for the purpose as a SERS tag noble metal nanosubstrate.

Conjugation Process

The optimization was primarily concerned with finding the optimal volume of PYOT to be used in the conjugation process. Too much added PYOT will cause the AuNPs to aggregate and crash out of solution, while too little PYOT would result in an ineffective SERS tag. Figure 18 outlines the optimization process of the conjugation optimization.

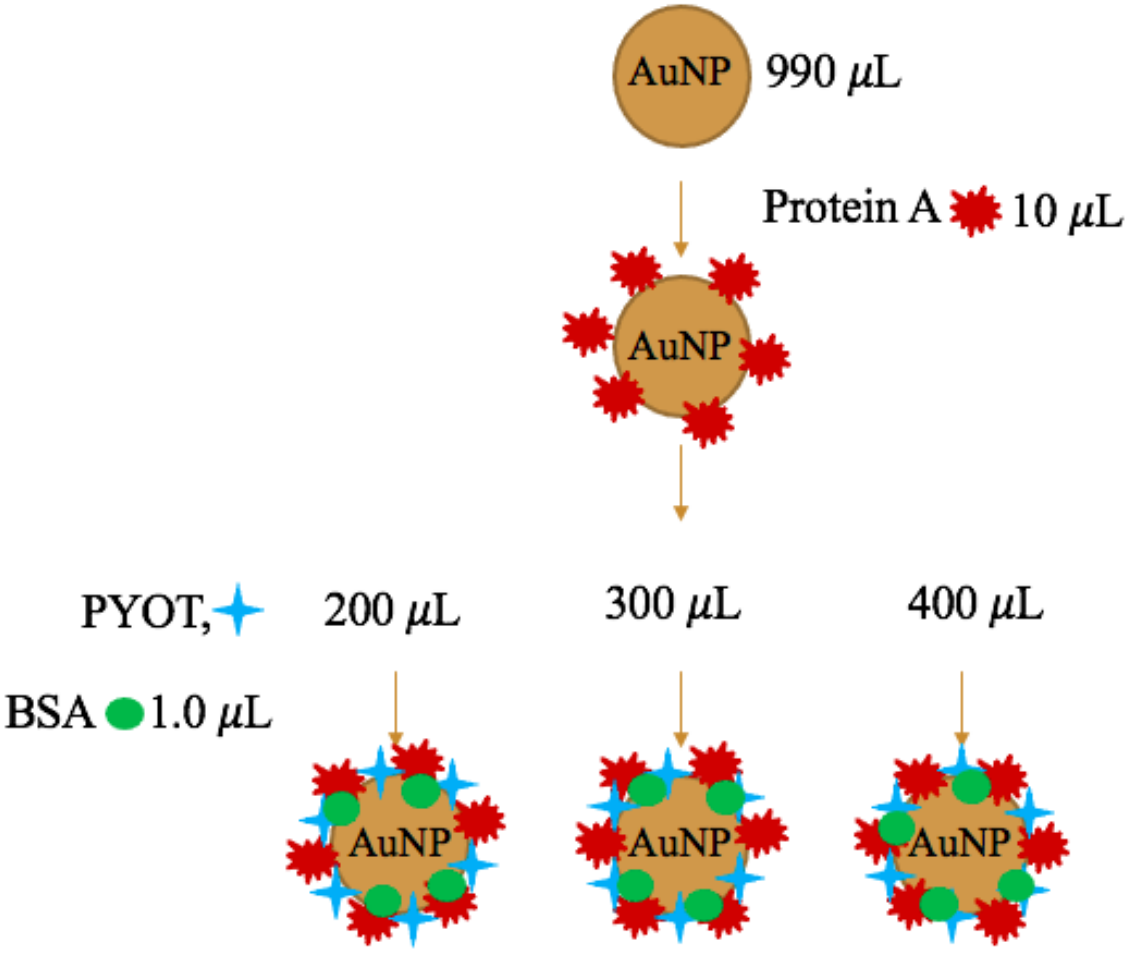

Figure 18. Outline of conjugation process. Varied PYOT volumes were explored while keeping other component volumes constant.

Various SERS and SEM analysis were obtained from samples at various stages in the conjugation process. These results were good indicators of the optimal PYOT volume to

use in the conjugation process. Based on SERS analysis, 400 μL PYOT was the optimal volume to use in the conjugation process. This PYOT amount offered the best SERS intensity and little interference. This is not an unexpected result, as Raman reporter molecules improve SERS signal, so an increased coating volume resulting in improved SERS signals and greater intensity is logical.

Additionally, samples were taken of the conjugation process solutions at a stage before and after the suspensions were centrifuged. The particle solutions offered improved SERS signals after they had been centrifuged, compared to the samples taken before being centrifuged. These SERS spectra can be found in Annex D, however, the results were obtained while the CCD was saturated and although gave some promising results, are unable to be accurately interpreted and need to be analysed further with a lower acquisition time. The increase in SERS signal after centrifugation is a result of AuNP aggregation, which results in the formation of many SERS-active “hot spots” where the local electromagnetic field is particularly enhanced.

Conclusion

SERS and SERS tag molecules offer important improvements in Raman spectroscopy and other research applications. Developing a particle from a conjugation process to act as a SERS tag is one important application of this research. The particle development, which has applications in SERS-based LFIA testing, will prove useful in future testing technology where LFIA tests may be considered. Since LFIA tests offer low sensitivity and selectivity on their own, SERS is an asset which improves both of the aforementioned disadvantages. SERS tag engineering is therefore a useful and active field of study. The SERS tag particle developed by the modified and optimized conjugation process offered promising results. The SERS spectra obtained from the final product offered good SERS signal intensity and consistent results, as well as spectra with few observable interferences.

Future Work

Particle stabilization must be verified and is a required future step before moving on to further studies using the SERS tag molecule in testing. First, the optimal AuNP size and PYOT amount used in the conjugation process must be verified. Once this has been completed, a fridge stabilization test should be performed. This would be performed by storing the optimized particles in a diluted solution for at least 10 days in the fridge. The particles would be deemed stable if after being removed from the fridge, the SERS signal were stable, and no aggregation or particle deposits are observed in the test container.

The particle comprised of gold conjugated to PYOT could be modified to include different constituents which may prove to be more optimal in SERS analysis and as a LFIA test particle. One modification could include replacing the PYOT Raman reporter molecule with an alternate Raman reporter for the purpose of potentially improving the SERS signal produced, particle stability, and LFIA test results. An alternate Raman reporter molecule to consider is 4-aminothiophenol (4-ATP). Ideal Raman reporter molecules have a high affinity to the noble metal nanosubstrate, so small thiolated molecules such as 4-ATP make appropriate choices. Along with having a high affinity for gold, 4-ATP is low cost, making it a practical Raman reporter molecule to test. Overall, these modifications could improve the performance of the test particle, or the original particle could be superior. It would be difficult to put confidence on one or the other. However, for the purpose of creating novel research, using the Raman reporter PYOT for the SERS tag would be ideal.

LFIA test kits are available for purchase and can be used to build an optimized test system. Optimal components could be chosen for the test by analyzing test particles with components using SERS and SEM, then comparing the results of the varied components of different materials and buffer treatments. Visual analysis of the test line results could also

be done comparing tests of different component and buffer types. The LFIA test kits available for purchase can be costly, which could hinder the ability to explore this option in the future.

In the case that the LFIA test kits are too costly to be used in research, store bought pregnancy tests may be purchased and modified to function as COVID-19 antibody tests. The target molecule of pregnancy tests is human Chorionic Gonadotrophin (hCG). In a positive pregnancy test result, hCG is trapped by a free hCG antibody, which has been attached to an enzyme dye, on the reaction site where the sample is placed. On the test line lies a fixed anti-hCG antibody, which is used to trap the hCG, which has previously been anchored to the free antibody and dye enzyme. The success of the anti-hCG antibody capturing hCG anchored to the free antibody and dye enzyme results in a positive test line being observed. In a negative pregnancy test result, hCG is not present in the sample, therefore hCG is not trapped by a free hCG antibody attached to an enzyme dye on the reaction site. The fixed antibody has no reaction without hCG. Therefore, no positive test line being observed. In both positive and negative test cases, the control line results to demonstrate a successful test. The control line of pregnancy tests contain a fixed anti-mouse IgG antibody attached to a dye enzyme, which binds to the free hCG antibody attached to dye enzyme from the reaction site, results in a visible line. In order to make these tests compatible with a SARS-CoV-2 antibody target molecule, the test lines would need to be modified. Figure 19 is a depiction of the proposed test line for a SERS-LFIA test to detect SARS-CoV-2 antibodies.

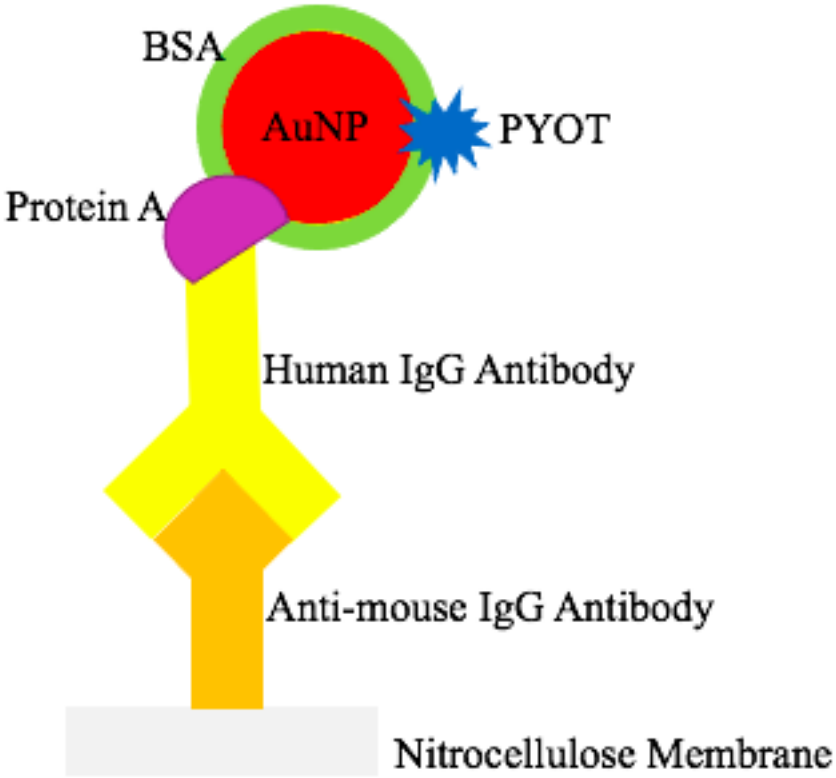

Figure 19. Proposed test line of SERS based LFIA test for antibodies including fixed and free antibodies, with the SERS tag molecule conjugated with the free Human IgG antibody for SARS-CoV-2.

Finally, multiple antibody types exist for SARS-CoV-2, including human IgG and IgM antibodies. A SERS-LFIA test could be created to test for multiple antibodies. This type of antibody test would contain multiple test lines, one for each antibody being tested, along with a control line.

Further analysis would be required before immediately swapping out test and control lines of store-bought pregnancy tests with test and control lines for SARS-CoV-2 antibodies. Fingerprinting methods such as Raman and IR spectroscopy could be used along with SEM to determine the chemical formulation of the test components of the store-bought tests. In particular, it would be important to determine the formulation of the sample pad containing the test and control lines. This would be important for identifying possible

interferences or other information which would make the test impractical for modification to a COVID-19 antibody test. Further, determining the treatment component parts may have had with buffers would be useful while considering test modifications.

An additional consideration for future work would be using the SERS-LFIA test analysis to quantify the antibody concentrations. Most current rapid testing technologies are LFIA tests which only provide a positive or negative result and are not quantitative. This is due in part to rapid testing requiring visual interpretation of results, since laboratory equipment required for more accurate and slower tests would not be available at pop-up rapid testing sites. Since a SERS-LFIA testing system would be developed, once the test has been completed, they could be analysed in a laboratory setting to provide antibody concentrations when positive results are indicated. Further, the option would exist to analyze negative tests, and if antibody concentrations are detected, it could be an indication that false negative visual results were obtained. The antibody concentrations could be found from the SERS signal results that would result from performing SERS analysis on the test spots.

References

(1) Bender, L. *Key Messages and Actions for COVID-19 Prevention and Control in Schools*; UNI220408; UNICEF: New York, 2020.

(2) World Health Organization. Coronavirus. https://www.who.int/health-topics/coronavirus#tab=tab_1 (accessed Apr 6, 2021).

(3) Centers for Disease Control and Prevention. People with Certain Medical Conditions. https://www.cdc.gov/coronavirus/2019-ncov/need-extra-precautions/people-with-medical-conditions.html (accessed Apr 6, 2021).

(4) World Health Organization. Transmission package: protect yourself and others from COVID-19. https://www.who.int/teams/risk-communication/covid-19-transmission-package (accessed Apr 6, 2021).

(5) Konda, A.; Prakash, A.; Moss, G. A.; Schmoldt, M.; Grant, G. D.; Guha, S. Aerosol Filtration Ffficiency of Common Fabrics Used in Respiratory Cloth Masks. *ACS Nano* **2020**, *14* (5), 6339–6347. https://doi.org/10.1021/acsnano.0c03252.

(6) Government of Canada. Moderna COVID-19 vaccine: What you should know. https://www.canada.ca/en/health-canada/services/drugs-health-products/covid19-industry/drugs-vaccines-treatments/vaccines/moderna.html (accessed Apr 6, 2021).

(7) Government of Canada. Pfizer-BioNTech COVID-19 vaccine: What you should know. https://www.canada.ca/en/health-canada/services/drugs-health-products/covid19-industry/drugs-vaccines-treatments/vaccines/pfizer-biontech.html (accessed Apr 6, 2021).

(8) Government of Canada. AstraZeneca COVID-19 vaccine: What you should know.

https://www.canada.ca/en/health-canada/services/drugs-health-products/covid19-industry/drugs-vaccines-treatments/vaccines/astrazeneca.html (accessed Apr 6, 2021).

(9) Government of Canada. Janssen COVID-19 vaccine: What you should know. https://www.canada.ca/en/health-canada/services/drugs-health-products/covid19-industry/drugs-vaccines-treatments/vaccines/janssen.html (accessed Apr 6, 2021).

(10) Kawasuji, H.; Takegoshi, Y.; Kaneda, M.; Ueno, A.; Miyajima, Y.; Kawago, K.; Fukui, Y.; Yoshida, Y.; Kimura, M.; Yamada, H.; Sakamaki, I.; Tani, H.; Morinaga, Y.; Yamamoto, Y. Transmissibility of COVID-19 Depends on the Viral Load around Onset in Adult and Symptomatic Patients. *PLoS One* **2020**, *15* (12), e0243597. https://doi.org/10.1371/journal.pone.0243597.

(11) Gandhi, M.; Rutherford, G. W. Facial Masking for Covid-19 — Potential for "Variolation" as We Await a Vaccine. *N. Engl. J. Med.* **2020**, *383* (18), e101. https://doi.org/10.1056/nejmp2026913.

(12) Cleveland Clinic. COVID-19 and PCR Testing. https://my.clevelandclinic.org/health/diagnostics/21462-covid-19-and-pcr-testing#:~:text=A polymerase chain reaction (PCR,you are no longer infected. (accessed Apr 6, 2021).

(13) Marshall, W. F. How do COVID-19 antibody tests differ from diagnostic tests? https://www.mayoclinic.org/diseases-conditions/coronavirus/expert-answers/covid-antibody-tests/faq-20484429 (accessed Apr 6, 2021).

(14) Government of Canada. Testing for COVID-19: Importance. https://www.canada.ca/en/public-health/services/diseases/2019-novel-coronavirus-infection/symptoms/testing.html (accessed Apr 6, 2021).

(15) Mayo Clinic. COVID-19 antibody testing. https://www.mayoclinic.org/tests-procedures/covid-19-antibody-testing/about/pac-20489696 (accessed Apr 6, 2021).

(16) Hagen, A. COVID-19 Serology Testing Explained. https://asm.org/Articles/2020/May/COVID-19-Serology-Testing-Explained (accessed Apr 6, 2021).

(17) Carter, L. J.; Garner, L. V.; Smoot, J. W.; Li, Y.; Zhou, Q.; Saveson, C. J.; Sasso, J. M.; Gregg, A. C.; Soares, D. J.; Beskid, T. R.; Jervey, S. R.; Liu, C. Assay Techniques and Test Development for COVID-19 Diagnosis. *ACS Cent. Sci.* **2020**, *6*, 591–605. https://doi.org/10.1021/acscentsci.0c00501.

(18) Wang, Y.; Yan, B.; Chen, L. SERS Tags: Novel Optical Nanoprobes for Bioanalysis. *Chem. Rev.* **2013**, *113* (3), 1391–1428. https://doi.org/10.1021/cr300120g.

(19) Cox, K. L.; Devanarayan, V.; Kriauciunas, A.; Manetta, J.; Montrose, C.; Sittampalam, S. Immunoassay Methods. In *Assay Guidance Manual*; Eli Lilly & Company and the National Center for Advancing Translational Sciences: Bethesda, Maryland.

(20) Zhao, Z.; Cui, H.; Song, W.; Ru, X.; Zhou, W.; Yu, X. *A Simple Magnetic Nanoparticles-Based Viral RNA Extraction Method for Efficient Detection of SARS-CoV-2*; 2020. https://doi.org/10.1101/2020.02.22.961268.

(21) Perez, J. M.; Simeone, F. J.; Saeki, Y.; Josephson, L.; Weissleder, R. Viral-Induced Self-Assembly of Magnetic Nanoparticles Allows the Detection of Viral Particles in Biological Media. *J. Am. Chem. Soc.* **2003**, *125* (34), 10192–10193. https://doi.org/10.1021/ja036409g.

(22) Wang, C.; Wang, C.; Wang, X.; Wang, K.; Zhu, Y.; Rong, Z.; Wang, W.; Xiao, R.;

Wang, S. Magnetic SERS Strip for Sensitive and Simultaneous Detection of Respiratory Viruses. *ACS Appl. Mater. Interfaces* **2019**, *11* (21), 19495–19505. https://doi.org/10.1021/acsami.9b03920.

(23) Wen, T.; Huang, C.; Shi, F. J.; Zeng, X. Y.; Lu, T.; Ding, S. N.; Jiao, Y. J. Development of a Lateral Flow Immunoassay Strip for Rapid Detection of IgG Antibody against SARS-CoV-2 Virus. *Analyst* **2020**, *145*, 5345–5352. https://doi.org/10.1039/d0an00629g.

(24) Maneeprakorn, W.; Bamrungsap, S.; Apiwat, C.; Wiriyachaiporn, N. Surface-Enhanced Raman Scattering Based Lateral Flow Immunochromatographic Assay for Sensitive Influenza Detection. *RSC Adv.* **2016**, *6*, 112079–112085. https://doi.org/10.1039/C6RA24418A.

(25) Tymm, C.; Zhou, J.; Tadimety, A.; Burklund, A.; Zhang, J. X. J. Scalable COVID-19 Detection Enabled by Lab-on-Chip Biosensors. *Cell. Mol. Bioeng.* **2020**, *13* (4), 313–329. https://doi.org/10.1007/s12195-020-00642-z.

(26) Vega, M. M.; Bonifacio, A.; Lughi, V.; Marsi, S.; Carrato, S.; Sergo, V. Long-Term Stability of Surfactant-Free Gold Nanostars. *J. Nanoparticle Res.* **2014**, *16*, 2729. https://doi.org/10.1007/s11051-014-2729-z.

(27) Bastús, N. G.; Comenge, J.; Puntes, V. Kinetically Controlled Seeded Growth Synthesis of Citrate-Stabilized Gold Nanoparticles of up to 200 Nm: Size Focusing versus Ostwald Ripening. *Langmuir* **2011**, *27* (17), 11098–11105. https://doi.org/10.1021/la201938u.

(28) Perrault, S. D.; Chan, W. C. W. Synthesis and Surface Modification of Highly Monodispersed, Spherical Gold Nanoparticles of 50-200 Nm. *J. Am. Chem. Soc.* **2009**, *131* (47), 17042–17043. https://doi.org/10.1021/ja907069u.

(29) Huang, C.; Wen, T.; Shi, F. J.; Zeng, X. Y.; Jiao, Y. J. Rapid Detection of IgM Antibodies against the SARS-CoV-2 Virus via Colloidal Gold Nanoparticle-Based Lateral-Flow Assay. *ACS Omega* **2020**, *5* (21), 12550–12556. https://doi.org/10.1021/acsomega.0c01554.

(30) Tomás, A. L.; de Almeida, M. P.; Cardoso, F.; Pinto, M.; Pereira, E.; Franco, R.; Matos, O. Development of a Gold Nanoparticle-Based Lateral-Flow Immunoassay for Pneumocystis Pneumonia Serological Diagnosis at Point-of-Care. *Front. Microbiol.* **2019**, *10*, 2917. https://doi.org/10.3389/fmicb.2019.02917.

(31) Xiao, R.; Lu, L.; Rong, Z.; Wang, C.; Peng, Y.; Wang, F.; Wang, J.; Sun, M.; Dong, J.; Wang, D.; Wang, L.; Sun, N.; Wang, S. Portable and Multiplexed Lateral Flow Immunoassay Reader Based on SERS for Highly Sensitive Point-of-Care Testing. *Biosens. Bioelectron.* **2020**, *168*, 112524. https://doi.org/10.1016/j.bios.2020.112524.

(32) Liu, H.; Dai, E.; Xiao, R.; Zhou, Z.; Zhang, M.; Bai, Z.; Shao, Y.; Qi, K.; Tu, J.; Wang, C.; Wang, S. Development of a SERS-Based Lateral Flow Immunoassay for Rapid and Ultra-Sensitive Detection of Anti-SARS-CoV-2 IgM/IgG in Clinical Samples. *Sensors Actuators, B Chem.* **2021**, *329*, 129196. https://doi.org/10.1016/j.snb.2020.129196.

(33) Clarke, O. J. R.; Goodall, B. L.; Hui, H. P.; Vats, N.; Brosseau, C. L. Development of a SERS-Based Rapid Vertical Flow Assay for Point-of-Care Diagnostics. *Anal. Chem.* **2017**, *89*, 1405–1410. https://doi.org/10.1021/acs.analchem.6b04710.

(34) Lyon, L. A.; Keating, C. D.; Fox, A. P.; Baker, B. E.; He, L.; Nicewarner, S. R.; Mulvaney, S. P.; Natan, M. J. Raman Spectroscopy. *Anal. Chem.* **1998**, *70* (12), 341–362. https://doi.org/10.1021/a1980021p.

(35) Roberts, J. D.; Caserio, M. C. 9.9: Raman Spectroscopy. https://chem.libretexts.org/Bookshelves/Organic_Chemistry/Book%3A_Basic_Principles_of_Organic_Chemistry_(Roberts_and_Caserio)/09%3A_Separation_Purification__Identification_of_Organic_Compounds/9.09%3A_Raman_Spectroscopy (accessed Apr 6, 2021).

(36) Osibanjo, R.; Curtis, R.; Lai, Z. Infrared Spectroscopy. https://chem.libretexts.org/Bookshelves/Physical_and_Theoretical_Chemistry_Textbook_Maps/Supplemental_Modules_(Physical_and_Theoretical_Chemistry)/Spectroscopy/Vibrational_Spectroscopy/Infrared_Spectroscopy/Infrared_Spectroscopy#:~:text=Introduction-,Infrared (IR) spectroscopy is one of the most common and,the ultraviolet and visible regions. (accessed Apr 6, 2021).

(37) Keresztury, G. Raman Spectroscopy: Theory. In *Handbook of Vibrational Spectroscopy*; Chalmers, J. M., Griffiths, P. R., Eds.; Major Reference Works; John Wiley & Sons, Inc., 2006. https://doi.org/https://doi.org/10.1002/0470027320.s0109.

(38) Mulvaney, S. P.; Keating, C. D. Raman Spectroscopy. *Anal. Chem.* **2000**, *72* (12), 145–158. https://doi.org/10.1021/a10000155.

(39) Bumbrah, G. S.; Sharma, R. M. Raman Spectroscopy – Basic Principle, Instrumentation and Selected Applications for the Characterization of Drugs of Abuse. *Egypt. J. Forensic Sci.* **2016**, *6* (3), 209–215. https://doi.org/10.1016/j.ejfs.2015.06.001.

(40) Rostron, P.; Gaber, S.; Gaber, D. Raman Spectroscopy, Review. *Int. J. Eng. Tech. Res.* **2016**, *6* (1), 50–64. https://www.erpublication.org/published_paper/IJETR042430.pdf

(41) Pence, I.; Mahadevan-Jansen, A. Clinical Instrumentation and Applications of Raman Spectroscopy. *Chem. Soc. Rev.* **2016**, *45* (7), 1958–1979. https://doi.org/10.1039/c5cs00581g.

(42) Blackie, E. J.; Le Ru, E. C.; Etchegoin, P. G. Single-Molecule Surface-Enhanced Raman Spectroscopy of Nonresonant Molecules. *J. Am. Chem. Soc.* **2009**, *131* (40), 14466–14472. https://doi.org/10.1021/ja905319w.

(43) Barbiellini, B. Enhancement of Raman Scattering from Molecules Placed near Metal Nanoparticles. *Low Temp. Phys.* **2017**, *43* (1), 159–161. https://doi.org/10.1063/1.4974193.

(44) Schatz, G. C.; Young, M. A.; Duyne, R. P. Van. Electromagnetic Mechanism of SERS. In *Surface-Enhanced Raman Scattering*; Kneipp, K., Moskovits, M., Kneipp, H., Eds.; Springer: Berlin, Heidelberg, 2006.

(45) Creighton, J. A.; Eadon, D. G. Ultraviolet-Visible Absorption Spectra of the Colloidal Metallic Elements. *J. Chem. Soc. Faraday Trans.* **1991**, *87* (24), 3881–3891. https://doi.org/10.1039/FT9918703881.

(46) Dörfer, T.; Schmitt, M.; Popp, J. Deep-UV Surface-Enhanced Raman Scattering. *J. Raman Spectrosc.* **2007**, *38* (11), 1379–1382. https://doi.org/10.1002/jrs.1831.

(47) Mock, J. J.; Barbic, M.; Smith, D. R.; Schultz, D. A.; Schultz, S. Shape Effects in Plasmon Resonance of Individual Colloidal Silver Nanoparticles. *J. Chem. Phys.* **2002**, *116* (15), 6755–6759. https://doi.org/10.1063/1.1462610.

(48) Aroca, R. *Surface-Enhanced Vibrational Spectroscopy*; John Wiley & Sons, Inc.: Chichester, West Sussex, England, 2007. https://doi.org/10.1002/9780470035641.

(49) Sharma, B.; Frontiera, R. R.; Henry, A.-I.; Ringe, E.; Van Duyne, R. P. SERS: Materials, Applications, and the Future Background and Mechanism. *Mater. Today* **2012**, *15* (1–2), 16–25. https://doi.org/10.1016/S1369-7021(12)70017-2

(50) Andreou, C.; Mirsafavi, R.; Moskovits, M.; Meinhart, C. D. Detection of Low Concentrations of Ampicillin in Milk. *Analyst* **2015**, *140* (15), 5003–5005. https://doi.org/10.1039/c5an00864f.

(51) Ayas, S.; Cinar, G.; Ozkan, A. D.; Soran, Z.; Ekiz, O.; Kocaay, D.; Tomak, A.; Toren, P.; Kaya, Y.; Tunc, I.; Zareie, H.; Tekinay, T.; Tekinay, A. B.; Guler, M. O.; Dana, A. Label-Free Nanometer-Resolution Imaging of Biological Architectures through Surface Enhanced Raman Scattering. *Sci. Rep.* **2013**, *3*, 2624. https://doi.org/10.1038/srep02624.

(52) Banaei, N.; Foley, A.; Houghton, J. M.; Sun, Y.; Kim, B. Multiplex Detection of Pancreatic Cancer Biomarkers Using a SERS-Based Immunoassay. *Nanotechnology* **2017**, *28* (45), 455101. https://doi.org/10.1088/1361-6528/aa8e8c.

(53) Fabris, L. Gold-Based SERS Tags for Biomedical Imaging. *J. Opt.* **2015**, *17* (11), 114002. https://doi.org/10.1088/2040-8978/17/11/114002.

(54) Gu, Y.; Zhang, Y.; Li, Y.; Jin, X.; Huang, C.; Maier, S. A.; Ye, J. Raman Photostability of Off-Resonant Gap-Enhanced Raman Tags. *RSC Adv.* **2018**, *8* (26), 14434–14444. https://doi.org/10.1039/c8ra02260g.

(55) Cialla, D.; März, A.; Böhme, R.; Theil, F.; Weber, K.; Schmitt, M.; Popp, J. Surface-Enhanced Raman Spectroscopy (SERS): Progress and Trends. *Anal. Bioanal. Chem.* **2012**, *403* (1), 27–54. https://doi.org/10.1007/s00216-011-5631-x.

(56) Kummitha, C. M.; Mayle, K. M.; Christman, M. A.; Deosarkar, S. P.; Schwartz, A. L.; McCall, K. D.; Kohn, L. D.; Malgor, R.; Goetz, D. J. A Sandwich ELISA for

the Detection of Wnt5a. *J. Immunol. Methods* **2010**, *352* (1–2), 38–44. https://doi.org/10.1016/j.jim.2009.11.005.

(57) Jentoft, F. C. Chapter 3 Ultraviolet–Visible–Near Infrared Spectroscopy in Catalysis: Theory, Experiment, Analysis, and Application Under Reaction Conditions. In *Advances in Catalysis*; Academic Press, 2009; pp 129–211.

(58) Limniou, M.; Papadopoulos, N.; Roberts, D. An Integrated Lecture, Virtual Instrumentation Lab Approach to Teaching UV-Vis Spectroscopy. *Educ. Inf. Technol.* **2007**, *12* (4), 229–244. https://doi.org/10.1007/s10639-007-9040-x.

(59) Misra, P., Dubinskii, M. *Ultraviolet Spectroscopy and UV Lasers*, 1st ed.; Misra, P., Dubinskii, M., Eds.; Taylor and Francis Group: Boca Raton, 2000.

(60) Amendola, V.; Meneghetti, M. Size Evaluation of Gold Nanoparticles by UV-Vis Spectroscopy. *J. Phys. Chem. C* **2009**, *113* (11), 4277–4285. https://doi.org/10.1021/jp8082425.

(61) Reimer, L. *Scanning Electron Microscopy*, 2nd ed.; Springer Verlag Berlin Heidelberg, 1998.

(62) Zhou, W.; Apkarian, R.; Wang, Z.; Joy, D. Fundamentals of Scanning Electron Microscopy (SEM). In *Scanning Microscopy for Nanotechnology*; Zhou, W., Wang, Z., Eds.; Springer: New York, 2006; pp 1–40.

(63) Nguyen, J. N.; Harbison, A. Scanning Electron Microscopy Sample Preparation and Imaging. In *Molecular Profiling. Methods in Molecular Biology*; Espina, V., Ed.; Springer: New York, 2017; pp 71–84.

(64) Koczula, K. M.; Gallotta, A. Lateral Flow Assays. *Essays Biochem.* **2016**, *60* (1), 111–120. https://doi.org/10.1042/EBC20150012.

(65) Sajid, M.; Kawde, A. N.; Daud, M. Designs, Formats and Applications of Lateral

Flow Assay: A Literature Review. *J. Saudi Chem. Soc.* **2015**, *19* (6), 689–705. https://doi.org/10.1016/j.jscs.2014.09.001.

Annex/Appendix

Annex A – SERS Analysis of AuNPs coated with PYOT using Cellulose Substrate

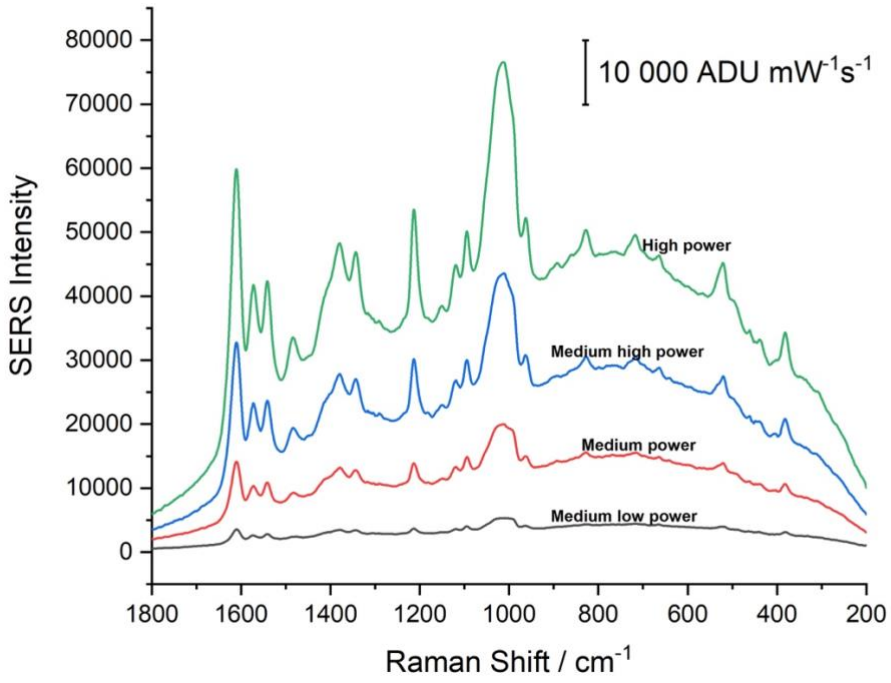

Figure 20. AuNP seed solution and PYOT on cellulose substrate offset at 2.93, 10.6, 22.3, 46.5, 55.9 mW laser powers at an acquisition time of 30 seconds.

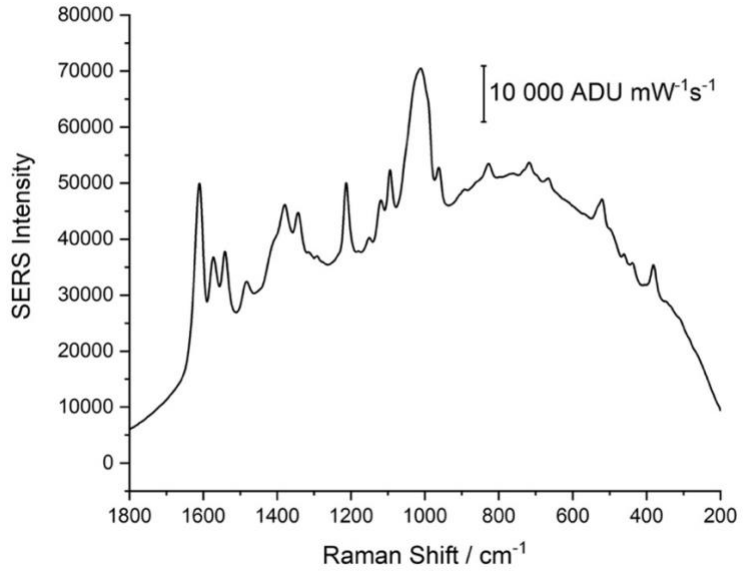

Figure 21. AuNP seed solution and PYOT on cellulose substrate 55.9 mW laser power 10 spots averaged at an acquisition time of 30 seconds.

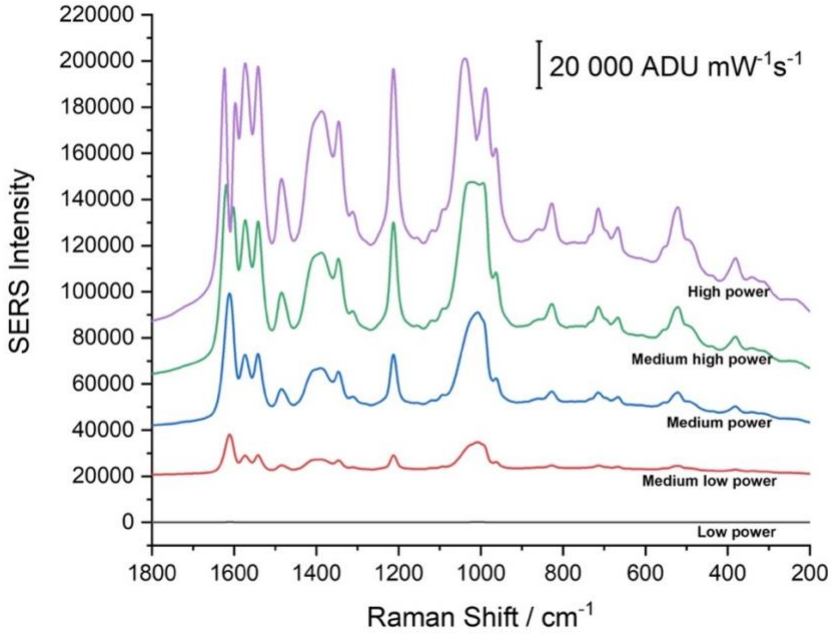

Figure 22. AuNP solution 1st dilution and PYOT on cellulose substrate offset at 2.93, 10.6, 22.3, 46.5, 55.9 mW laser powers at an acquisition time of 30 seconds.

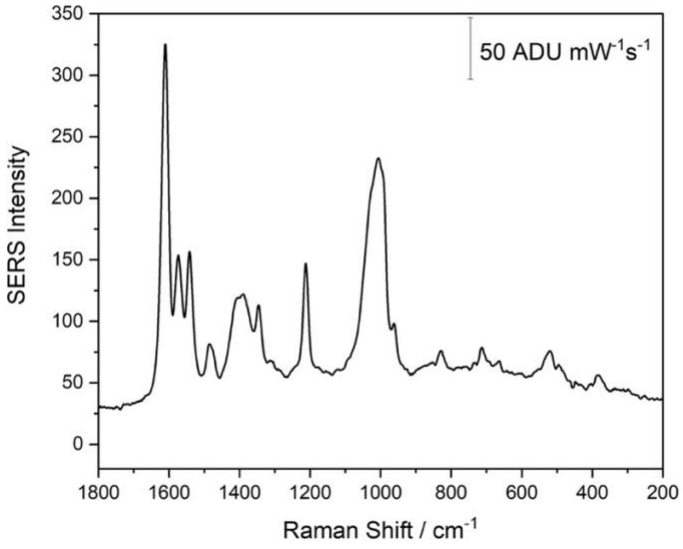

Figure 23. AuNP solution 1st dilution and PYOT on cellulose substrate 2.93 mW laser power 10 spots averaged at an acquisition time of 30 seconds.

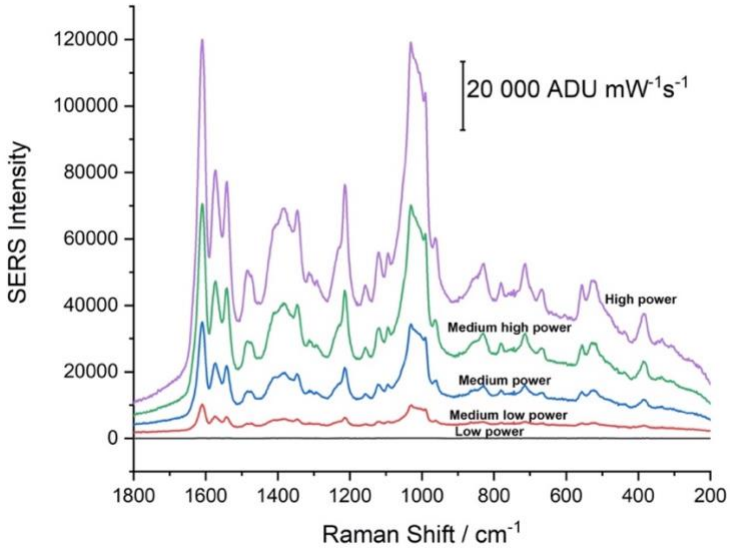

Figure 24. AuNP solution 2nd dilution and PYOT on cellulose substrate offset at 2.93, 10.6, 22.3, 46.5, 55.9 mW laser powers at an acquisition time of 30 seconds.

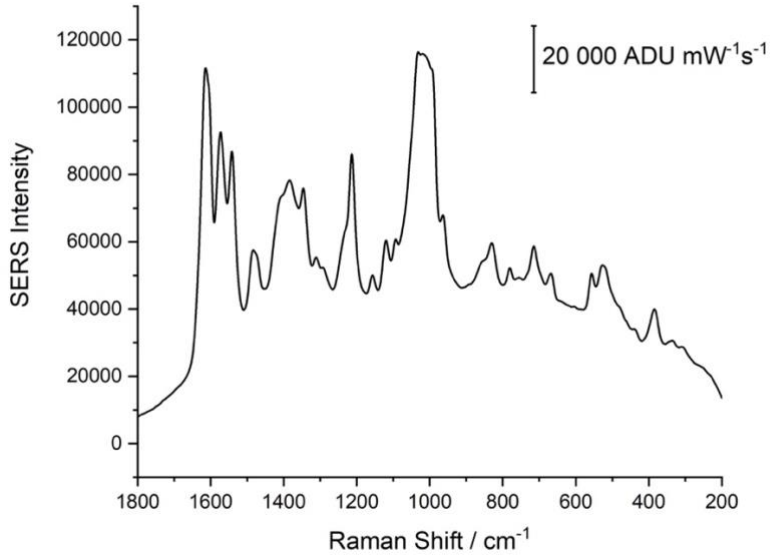

Figure 25. AuNP solution 2nd dilution and PYOT on cellulose substrate 55.9 mW laser power 10 spots averaged at an acquisition time of 30 seconds.

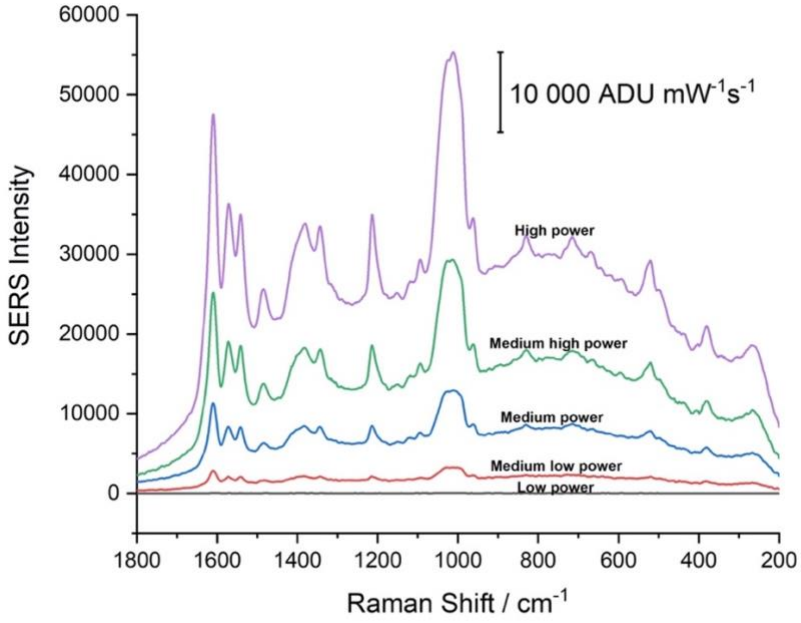

Figure 26. AuNP solution 3rd dilution and PYOT on cellulose substrate offset at 2.93, 10.6, 22.3, 46.5, 55.9 mW laser powers at an acquisition time of 30 seconds.

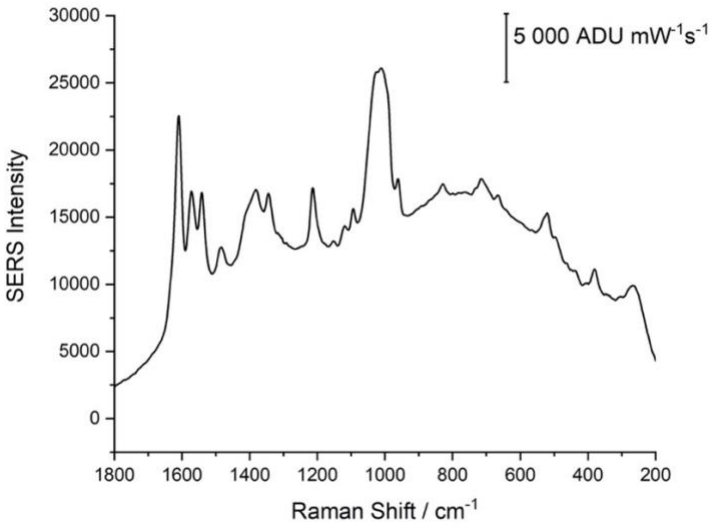

Figure 27. AuNP solution 3rd dilution and PYOT on cellulose substrate 10.6 mW laser power 10 spots averaged at an acquisition time of 30 seconds.

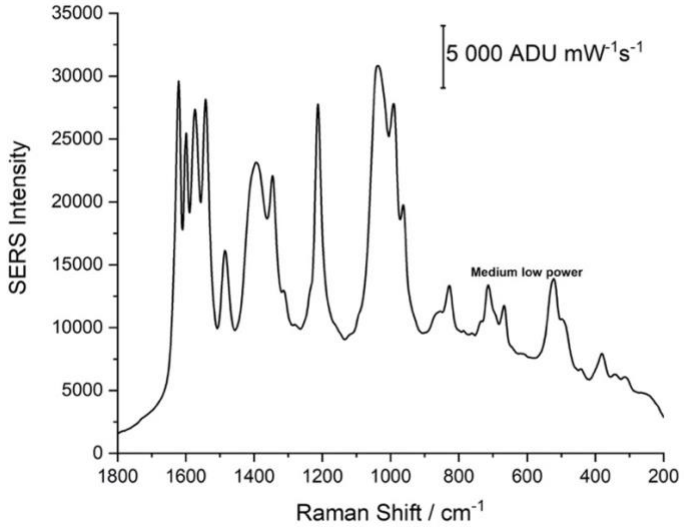

Figure 28. AuNP solution 4th dilution and PYOT on cellulose substrate offset at 22.3 mW laser power at an acquisition time of 30 seconds. All higher attempted laser powers gave saturated results.

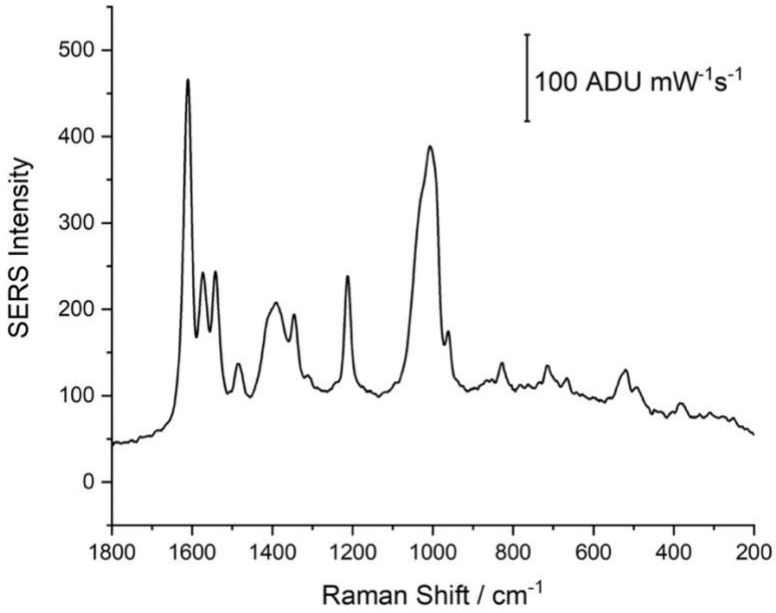

Figure 29. AuNP solution 4th dilution and PYOT on cellulose substrate 2.93 mW laser power 10 spots averaged at an acquisition time of 30 seconds.

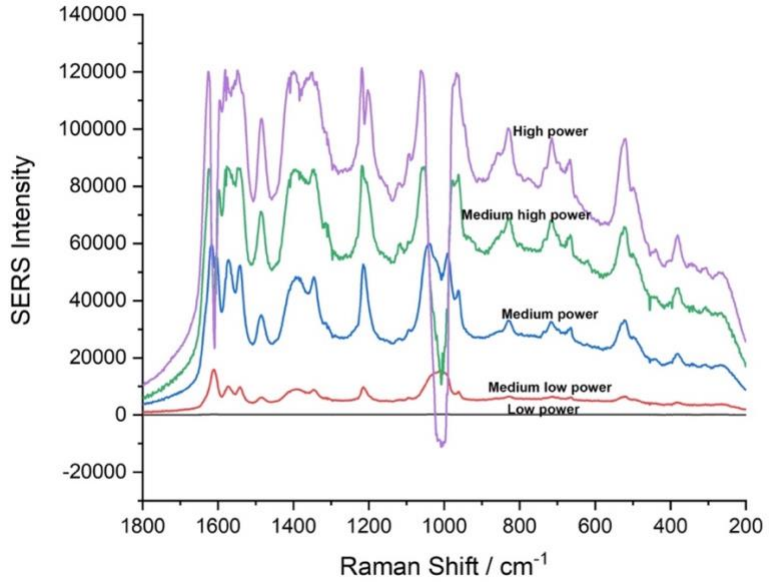

Figure 30. AuNP solution 5th dilution and PYOT on cellulose substrate offset at 2.93, 10.6, 22.3, 46.5, 55.9 mW laser powers at an acquisition time of 30 seconds. This spectrum shows an example of a saturated CCD where spectral interpretation is not possible.

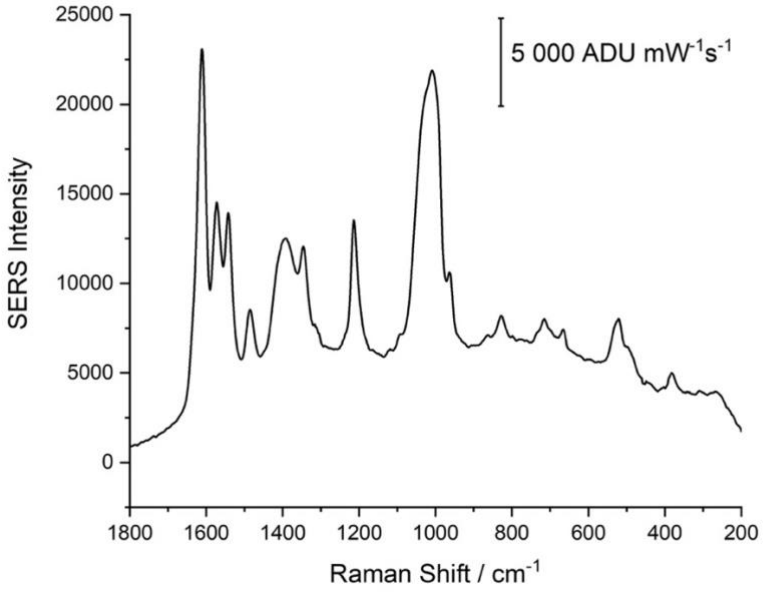

Figure 31. AuNP solution 5th dilution and PYOT on cellulose substrate 10.6 mW laser power 10 spots averaged at an acquisition time of 30 seconds.

Annex B – SERS Analysis of AuNP coated with PYOT using Nitrocellulose Substrate

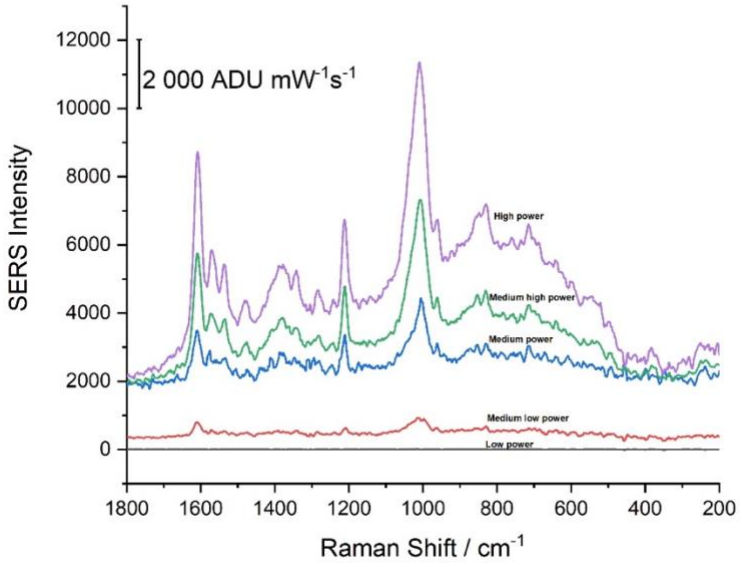

Figure 32. AuNP seed solution and PYOT on nitrocellulose substrate offset at 2.93, 10.6, 22.3, 46.5, 55.9 mW laser powers at an acquisition time of 30 seconds.

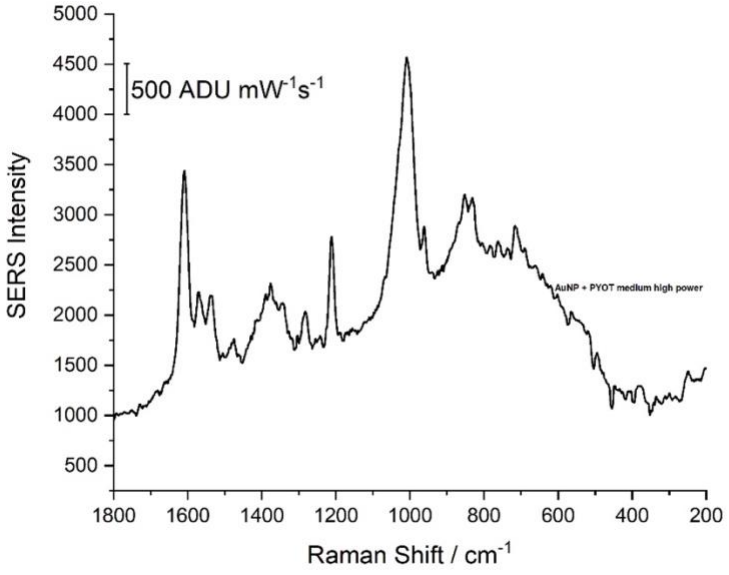

Figure 33. AuNP seed solution and PYOT on nitrocellulose substrate at 46.5 mW laser power 10 spots averaged at an acquisition time of 30 seconds.

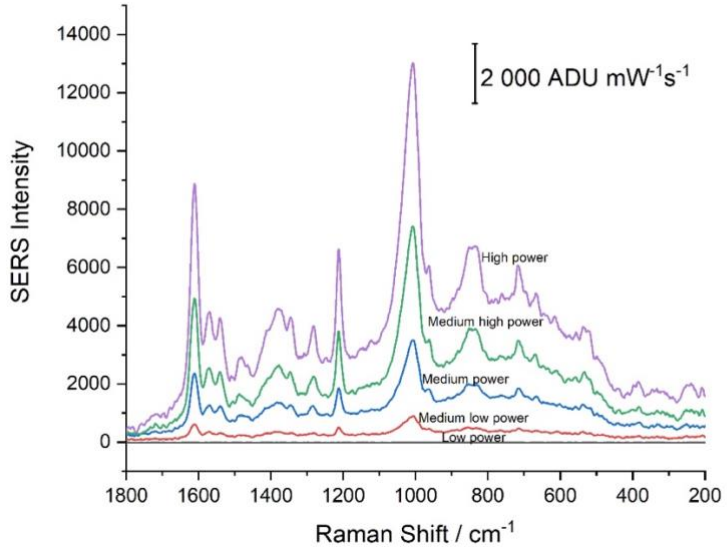

Figure 34. AuNP 1st dilution and PYOT on nitrocellulose substrate offset at 2.93, 10.6, 22.3, 46.5, 55.9 mW laser powers at an acquisition time of 30 seconds.

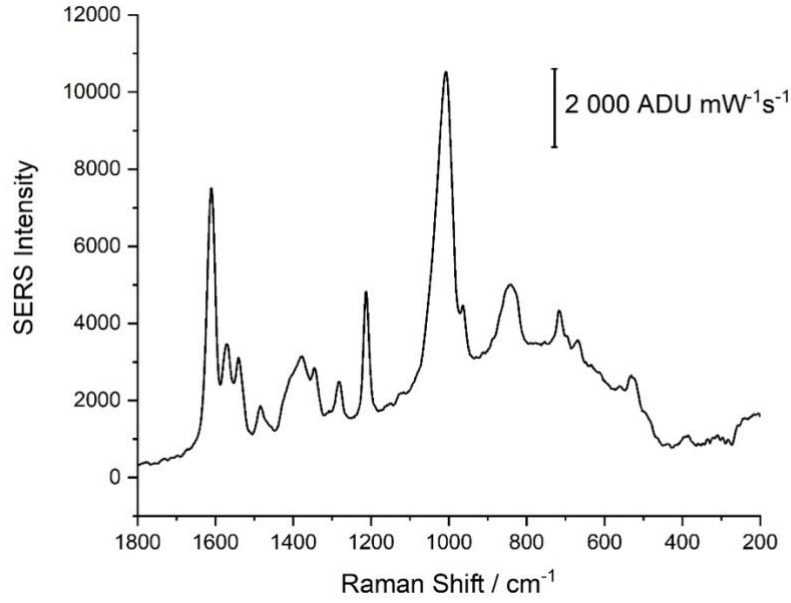

Figure 35. AuNP 1st dilution and PYOT on nitrocellulose substrate at 55.9 mW laser power 10 spots averaged at an acquisition time of 30 seconds.

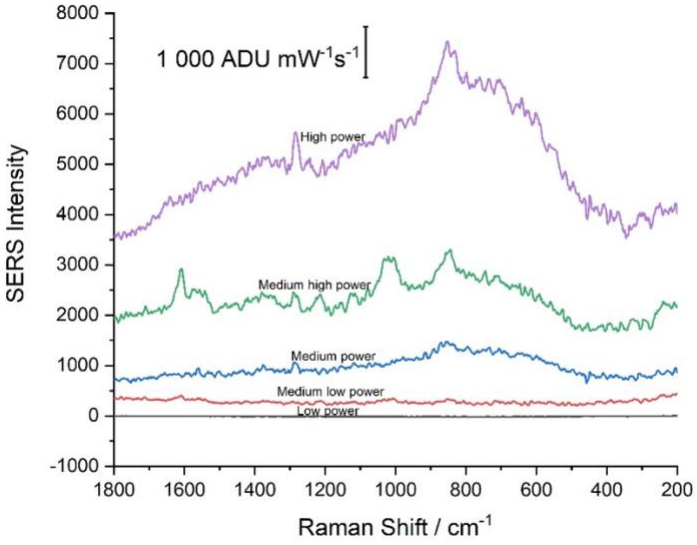

Figure 36. AuNP 2nd dilution and PYOT on nitrocellulose substrate offset at 2.93, 10.6, 22.3, 46.5, 55.9 mW laser powers at an acquisition time of 30 seconds.

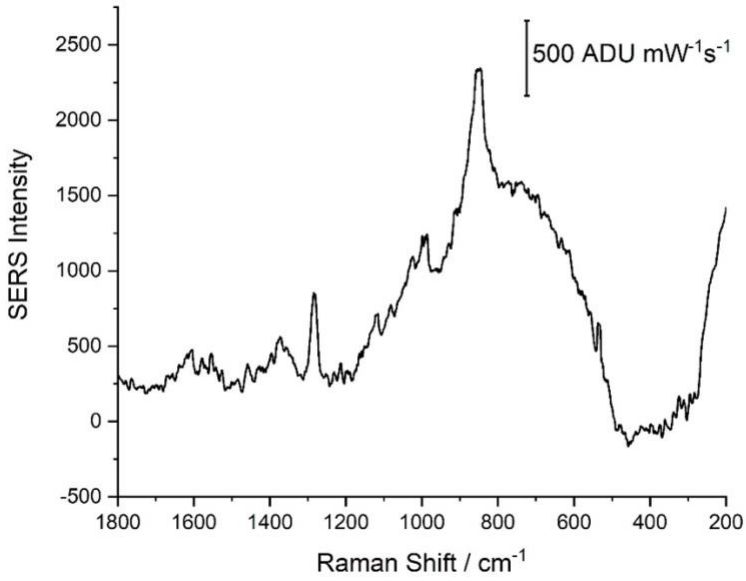

Figure 37. AuNP 2nd dilution and PYOT on nitrocellulose substrate at 55.9 mW laser power 10 spots averaged at an acquisition time of 30 seconds.

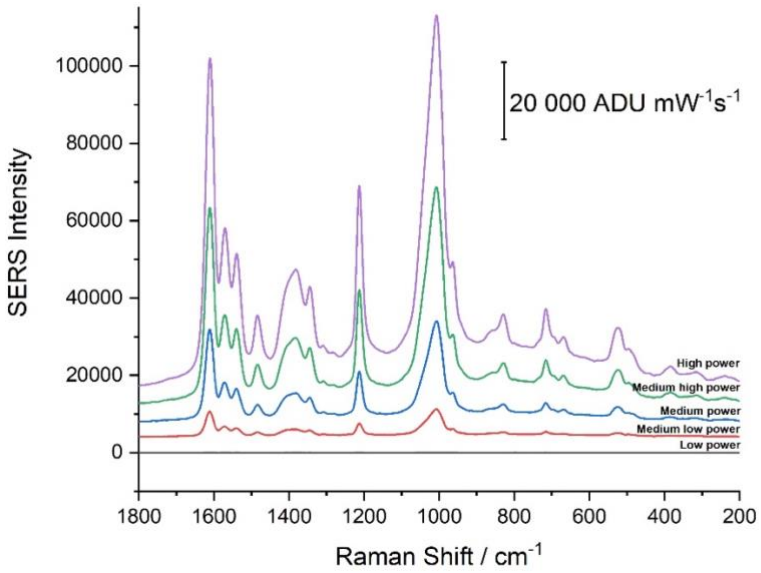

Figure 38. AuNP 3rd dilution and PYOT on nitrocellulose substrate offset at 2.93, 10.6, 22.3, 46.5, 55.9 mW laser powers at an acquisition time of 30 seconds.

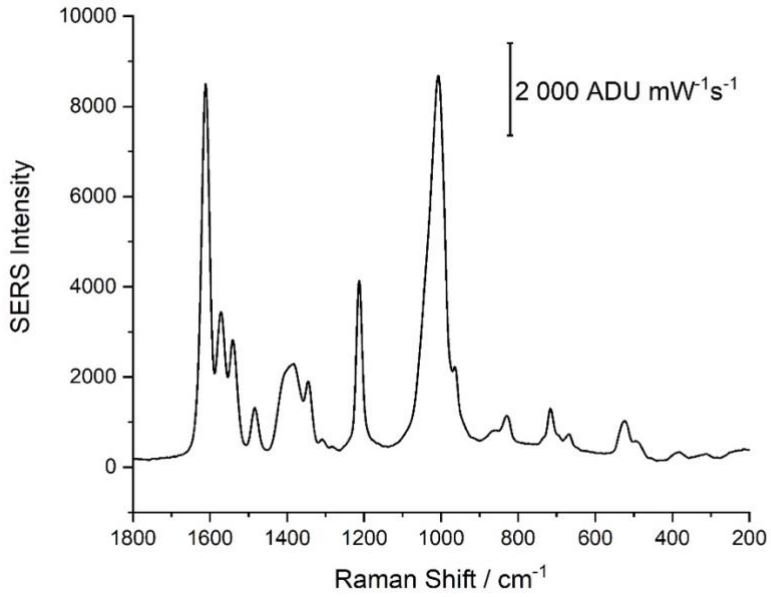

Figure 39. AuNP 3rd dilution and PYOT on nitrocellulose substrate at 10.6 mW laser power 10 spots averaged at an acquisition time of 30 seconds.

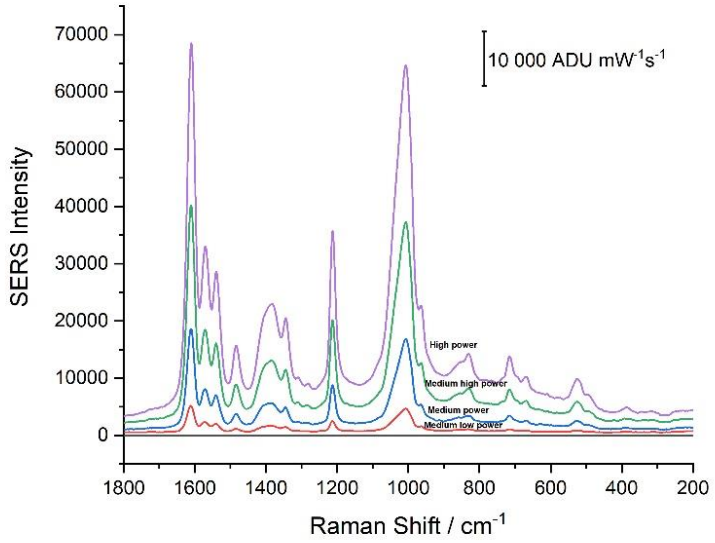

Figure 40. AuNP 4th dilution and PYOT on nitrocellulose substrate offset at 2.93, 10.6, 22.3, 46.5, 55.9 mW laser powers at an acquisition time of 30 seconds.

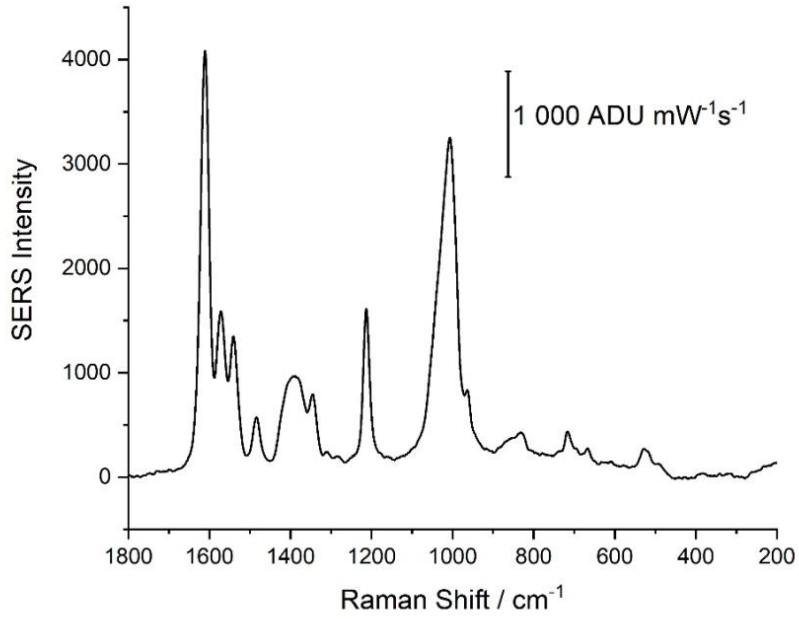

Figure 41. AuNP 4th dilution and PYOT on nitrocellulose substrate at 10.6 mW laser power 10 spots averaged at an acquisition time of 30 seconds.

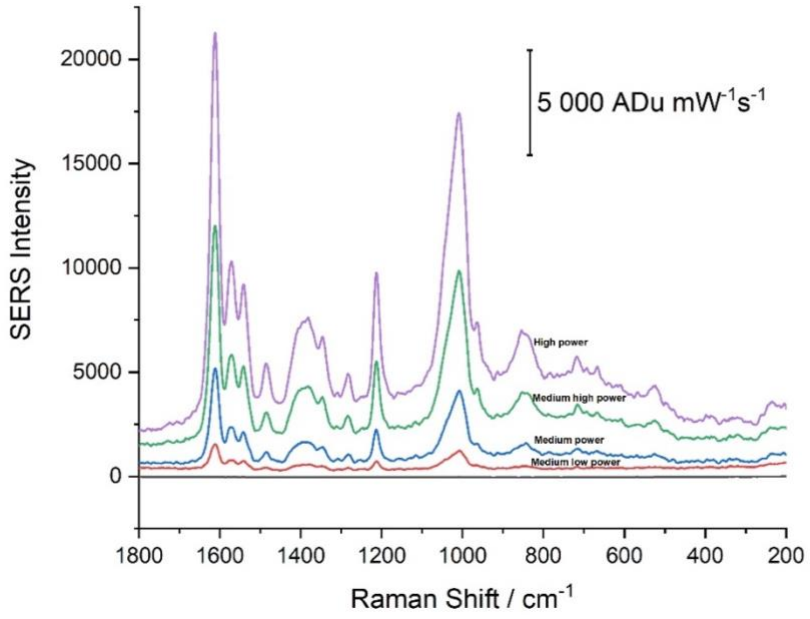

Figure 42. AuNP 5th dilution and PYOT on nitrocellulose substrate offset at 2.93, 10.6, 22.3, 46.5, 55.9 mW laser powers at an acquisition time of 30 seconds.

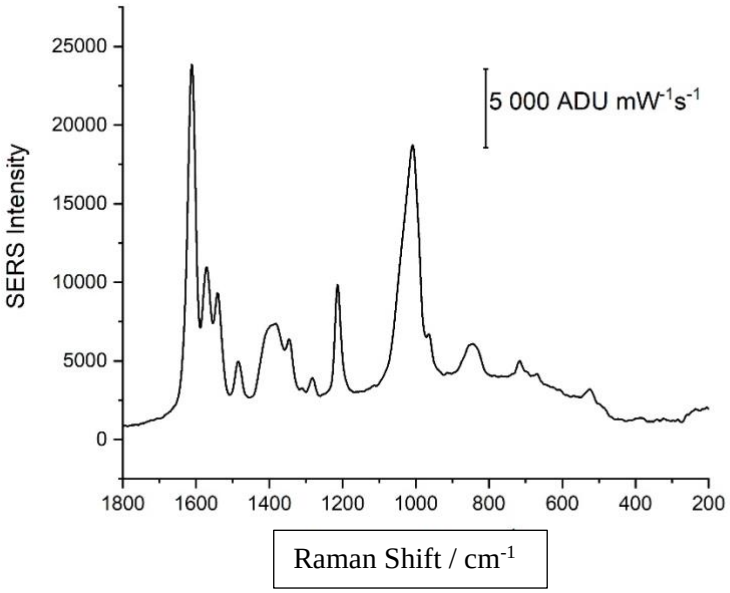

Figure 43. AuNP 5th dilution and PYOT on nitrocellulose substrate at 55.9 mW laser power 10 spots averaged at an acquisition time of 30 seconds.

Annex C – IgG Activity Tests Including Various Dilution Factors using Cellulose Substrate

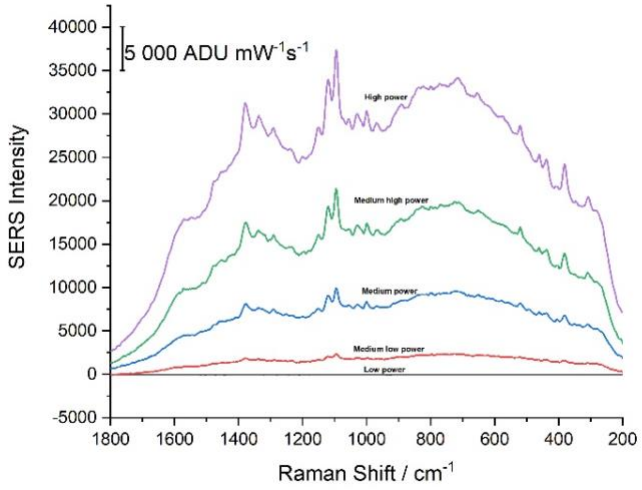

Figure 44. IgG activity control test without a dilution factor of the conjugated Protein A-AuNP solution offset at 2.93, 10.6, 22.3, 46.5, 55.9 mW laser powers at an acquisition time of 30 seconds.

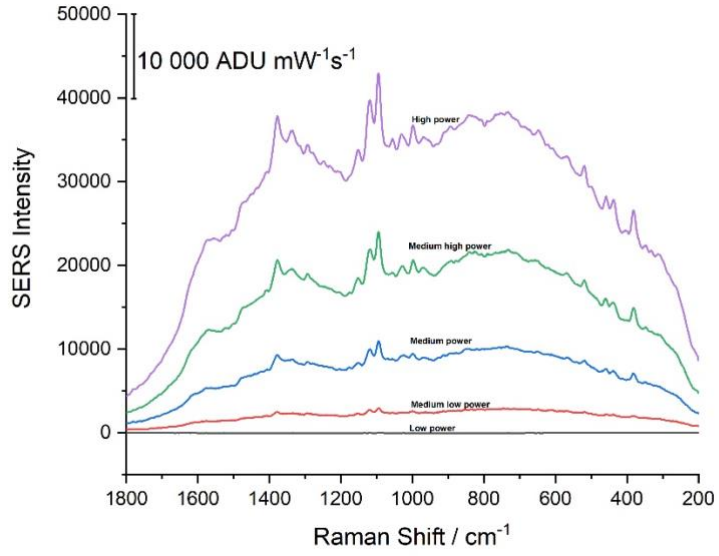

Figure 45. IgG solution activity test without a dilution factor of the conjugated Protein A-AuNP solution offset at 2.93, 10.6, 22.3, 46.5, 55.9 mW laser powers at an acquisition time of 30 seconds.

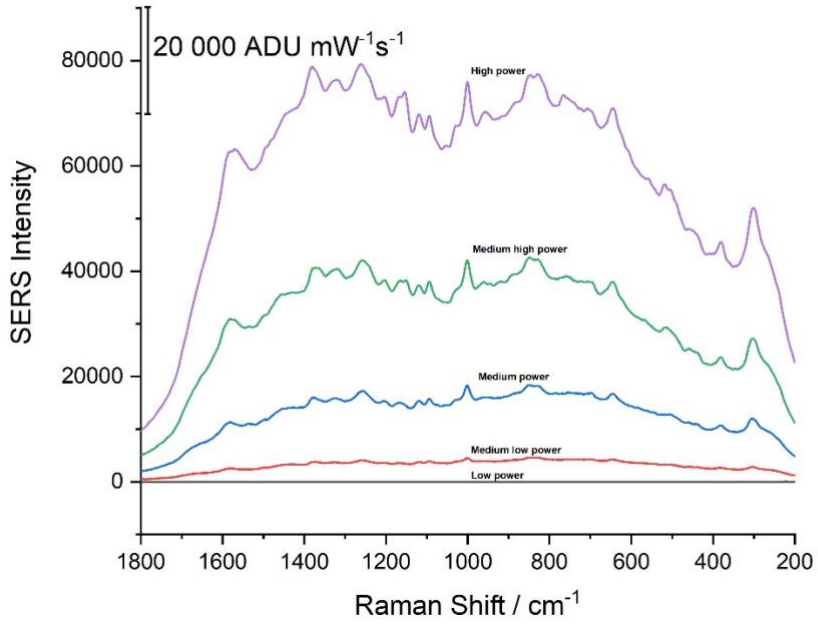

Figure 46. IgG activity saliva test without a dilution factor of the conjugated Protein A-AuNP solution offset at 2.93, 10.6, 22.3, 46.5, 55.9 mW laser powers at an acquisition time of 30 seconds.

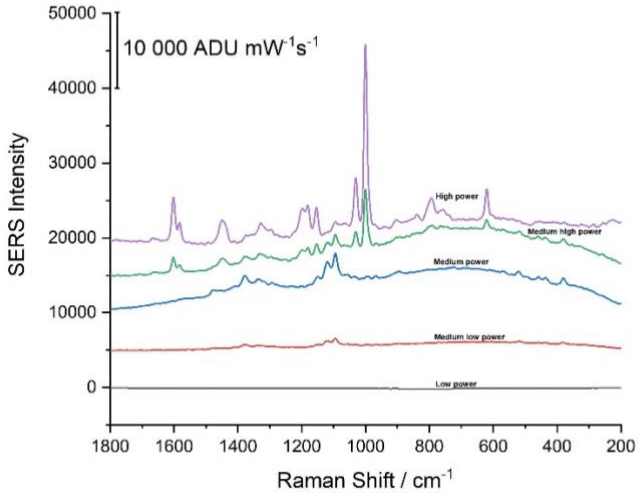

Figure 47. IgG activity control test with a dilution factor of 3 of the conjugated Protein A-AuNP solution offset at 2.93, 10.6, 22.3, 46.5, 55.9 mW laser powers at an acquisition time of 30 seconds.

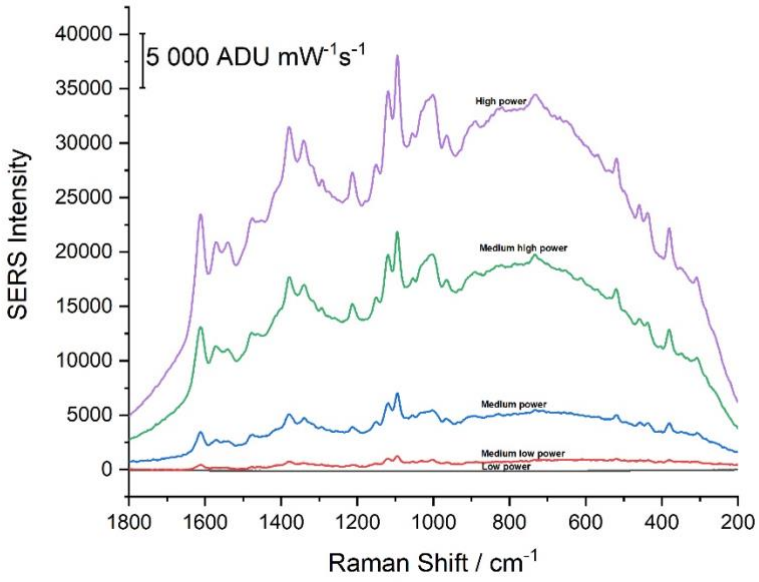

Figure 48. IgG solution activity test with a dilution factor of 3 of the conjugated Protein A-AuNP solution offset at 2.93, 10.6, 22.3, 46.5, 55.9 mW laser powers at an acquisition time of 30 seconds.

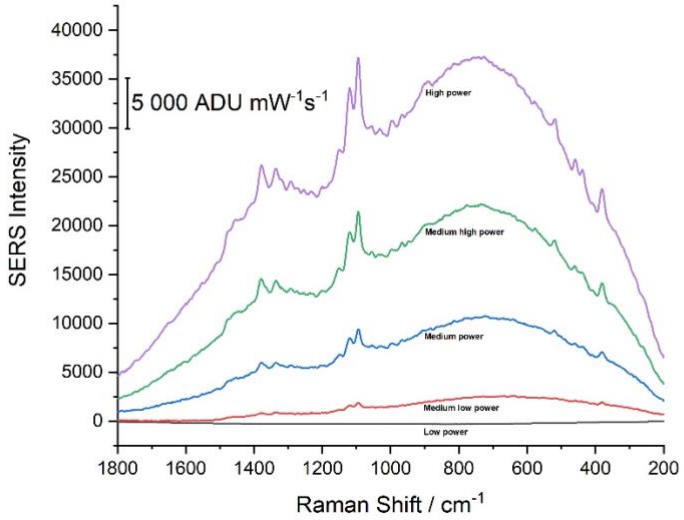

Figure 49. IgG activity saliva test with a dilution factor of 3 of the conjugated Protein A-AuNP solution offset at 2.93, 10.6, 22.3, 46.5, 55.9 mW laser powers at an acquisition time of 30 seconds.

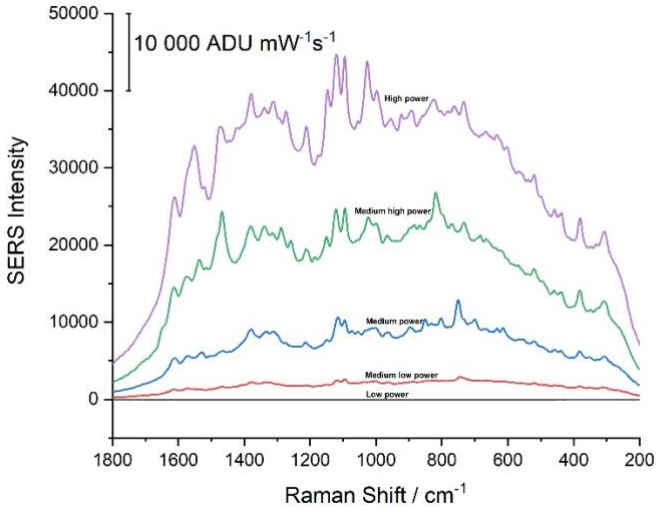

Figure 50. IgG activity control test with a dilution factor of 6 of the conjugated Protein A-AuNP solution offset at 2.93, 10.6, 22.3, 46.5, 55.9 mW laser powers at an acquisition time of 30 seconds.

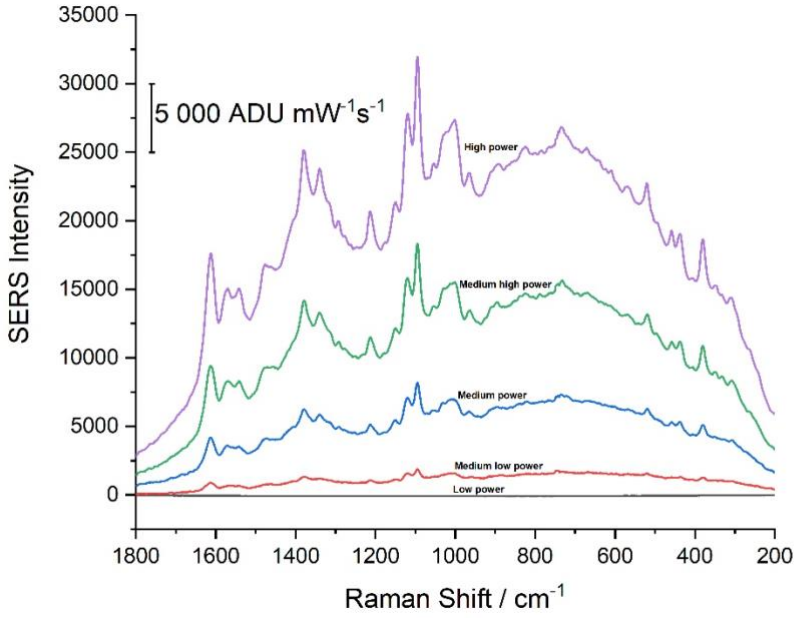

Figure 51. IgG solution activity test with a dilution factor of 6 of the conjugated Protein A-AuNP solution offset at 2.93, 10.6, 22.3, 46.5, 55.9 mW laser powers at an acquisition time of 30 seconds.

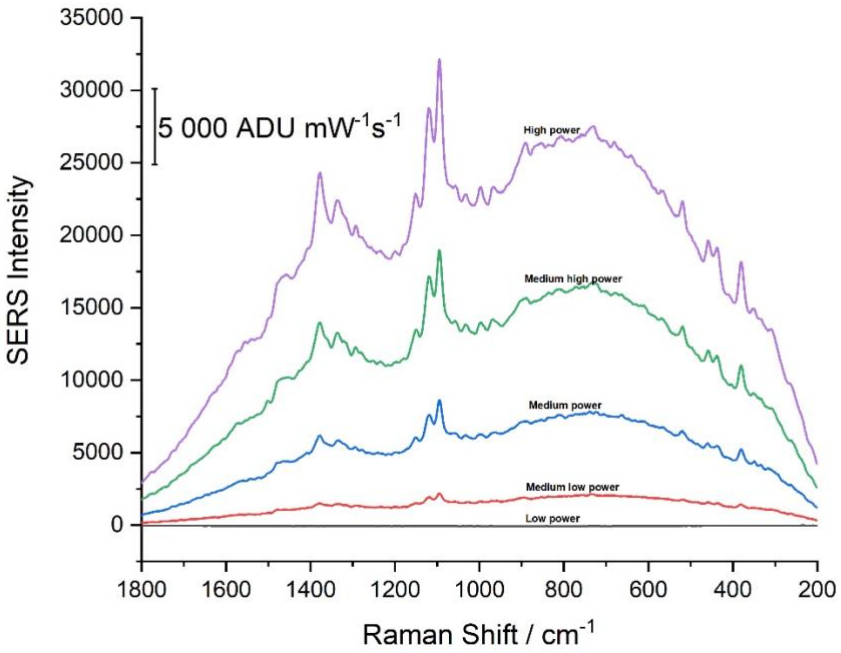

Figure 52. IgG activity saliva test with a dilution factor of 6 of the conjugated Protein A-AuNP solution offset at 2.93, 10.6, 22.3, 46.5, 55.9 mW laser powers at an acquisition time of 30 seconds.

.

Annex D – SERS Analysis of Conjugation Process

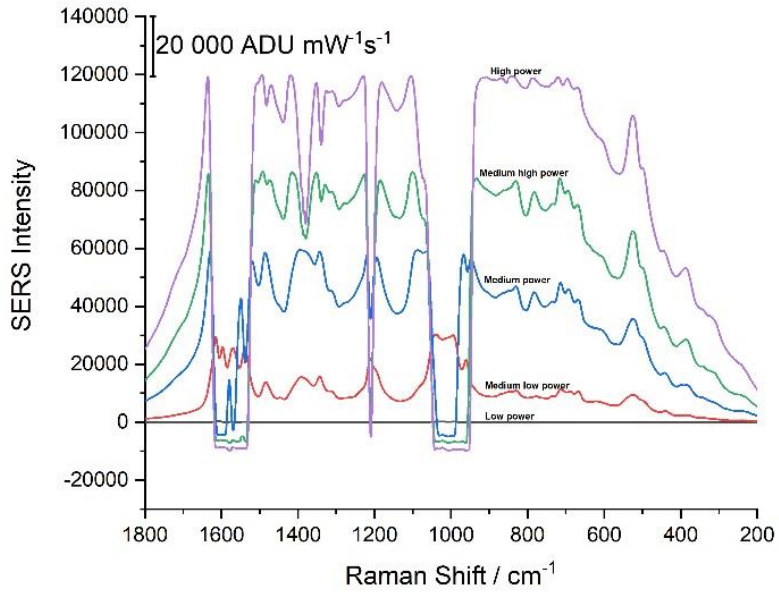

Figure 53. Preliminary conjugation results obtained before the centrifuge step in the conjugation process, with 400 µL PYOT used. This shows an offset at 2.93, 10.6, 22.3, 46.5, 55.9 mW laser powers at an acquisition time of 30 seconds.

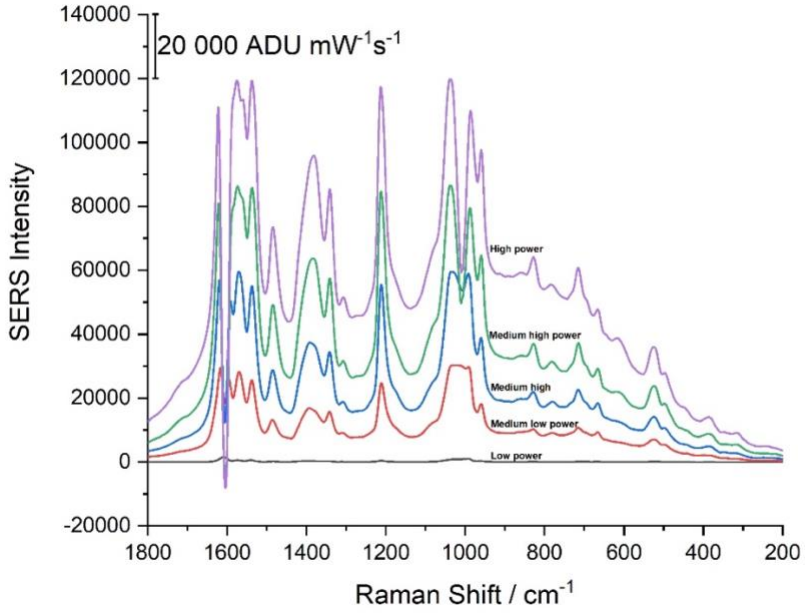

Figure 54. Conjugation results obtained after the centrifuge step, with 400 μL PYOT used. This shows an offset at 2.93, 10.6, 22.3, 46.5, 55.9 mW laser powers at an acquisition time of 30 seconds. These results cannot be interpreted due to the CCD being saturated.